

# Small scale induced gravitational waves from primordial black holes, a stringent lower mass bound, and the imprints of an early matter to radiation transition

Nilanjandev Bhaumik<sup>\*</sup> and Rajeev Kumar Jain<sup>†</sup>

*Department of Physics, Indian Institute of Science, Bangalore 560012, India*

 (Received 15 April 2021; accepted 9 July 2021; published 28 July 2021)

In all inflationary scenarios of primordial black hole (PBH) formation, amplified scalar perturbations inevitably accompany an induced stochastic gravitational wave background (ISGWB) at smaller scales. In this paper, we study the ISGWB originating from the inflationary model, introduced in our previous paper [N. Bhaumik and R. K. Jain, Primordial black holes dark matter from inflection point models of inflation and the effects of reheating, *J. Cosmol. Astropart. Phys.* **01** (2020) 037] wherein PBHs can be produced with a nearly monochromatic mass fraction in the asteroid mass window accounting for the total dark matter in the universe. We numerically calculate the ISGWB in our scenario for frequencies ranging from nano-Hz to kHz that covers the observational scales corresponding to future space-based gravitational wave (GW) observatories such as IPTA, LISA, DECIGO, and Einstein Telescope. Interestingly, we find that ultralight PBHs ( $M_{\text{PBH}} \sim 10^{-20} M_{\odot}$ ), which shall completely evaporate by today with an exceedingly small contribution to dark matter, would still generate an ISGWB that may be detected by a future design of the ground-based Advanced LIGO detector. Using a model-independent approach, we obtain a stringent lower mass limit for ultralight PBHs which would be valid for a large class of ultra slow roll inflationary models. Further, we extend our formalism to study the imprints of a reheating epoch on both the ISGWB and the derived lower mass bound. We find that any noninstantaneous reheating leads to an even stronger lower bound on the PBH mass and an epoch of a prolonged matter-dominated reheating shifts the ISGWB spectrum to smaller frequencies. In particular, we show that an epoch of an early matter-dominated phase leads to a secondary amplification of the ISGWB at a much smaller scale corresponding to the smallest comoving scale leaving the horizon during inflation or the end of the inflation scale. Finally, we discuss the prospects of the ISGWB detection by the proposed and upcoming GW observatories.

DOI: [10.1103/PhysRevD.104.023531](https://doi.org/10.1103/PhysRevD.104.023531)

## I. INTRODUCTION

Primordial black holes (PBH) are now widely considered one of the most interesting candidates to explain the cold dark matter (CDM) in the universe and have gained a lot of attention lately, thanks to the recent detection of astrophysical gravitational waves (GW) from a system of binary black holes, as reported by the LIGO-Virgo scientific collaboration [1–6]. Moreover, it has been discussed that supermassive black holes which are observed at the center of massive galaxies at high redshifts could have been originated from the distribution of PBHs [7–10]. It is well known that PBHs can be produced in the early universe, particularly after inflation when primordial curvature perturbations with large overdensities reenter the horizon during the radiation dominated (RD) epoch [11–14]. Lately, a large number of inflationary models have been studied to produce PBHs in different mass ranges, in

particular, the class of models producing PBHs in the asteroid mass window in which PBHs could contribute to the total CDM in the universe [15–39].

A stochastic background of primordial GWs is a central prediction of all the inflationary models. In particular, a nearly scale invariant spectrum of tensor perturbations is widely regarded as the holy grail of canonical single field slow roll inflationary models. Such a background encodes pivotal information which can be used to probe and constrain the physics of the early universe and fundamental physics operating at very high energies. In single field slow roll inflationary models, the nearly scale invariant GW background is usually generated from the amplification of vacuum tensor fluctuations at the linear order wherein the inflaton field is the only dynamical degree of freedom. However, models with many dynamical fields such as extra spectator fields or gauge fields also lead to a secondary background of GWs with very different properties and characteristics than the vacuum contribution. Distinct signatures of such a background can then be used to probe a general class of inflationary scenarios beyond the single

<sup>\*</sup>nilanjandev@iisc.ac.in  
<sup>†</sup>rkjain@iisc.ac.in

field inflationary models. Besides probing the fundamental physics of the early universe, the spectral energy density of inflationary GWs at the present epoch can also be used to trace and probe the thermal history of the universe [40–46]. For some recent reviews on various cosmological backgrounds of GWs, their generation, and their detection, see Refs. [47,48].

In general, an induced stochastic gravitational wave background (ISGWB) at second order through mode coupling of scalar metric perturbations is always generated in all the inflationary models. Since the power spectrum of second-order metric perturbations should be of order  $10^{-18}$  in the RD era, one can expect this GW background to be extremely small and quite far from the reach of present and upcoming GW observatories. However, in all the inflationary scenarios of PBH formation, since the power spectrum of scalar curvature perturbations must be enhanced to  $\sim 10^{-2}$  at smaller scales to produce PBHs, this ISGWB typically turns out to be quite large and is, therefore, considered an interesting and relevant byproduct of all such inflationary scenarios [49–68].

In an earlier paper [69], we had studied an inflationary scenario with a sixth-order polynomial potential that allows the existence of an inflection point in the inflaton potential. Such a potential allows an epoch of an ultra slow roll (USR) evolution which leads to an enhancement of the spectrum of primordial scalar curvature perturbations at small scales. We found that this scenario can produce PBHs in different mass ranges and, in particular, in the asteroid mass range in which PBHs can contribute to the entire CDM. In this paper, we shall study the ISGWB arising in this scenario which is generated from the contribution due to mode coupling of first-order scalar perturbations at quadratic order. Such GWs are generated on smaller scales after they reenter the horizon during the RD phase. We shall calculate this ISGWB in our model, which is produced in a range of different frequencies from nano-Hz to kHz, using an adequate numerical approach and we will compare it with the current and projected sensitivities of various ground- and future space-based GW observatories. Interestingly, we find that in our model this ISGWB can be simultaneously detected by different GW observatories, which is usually not the case when the primordial power spectrum is highly peaked. We emphasize that this feature provides a unique opportunity to constrain the resulting signal much better. In models which produce PBHs in the asteroid mass window as in our scenario, the secondary GW background is usually peaked in the frequency band  $f_{\text{GW}} \sim 10^{-3} - 1$  Hz and thus can be potentially detected by the future space-based GW observatories such as LISA [70–73], TAIJI [74], DECIGO [75,76], or BBO [77]. Moreover, we notice an interesting observational possibility that ultralight PBHs produced in our scenario with mass  $M_{\text{PBH}} \sim 10^{-20} - 10^{-21} M_{\odot}$ , which would have been completely evaporated by today, would still lead to an ISGWB at larger frequencies which can, in

principle, be observed by the future design of the ground-based Advanced LIGO detector [78].

Furthermore, using a model-independent approach, we obtain a robust lower bound on the PBH mass in our case by assuming an instantaneous as well as a smooth transition from the USR to the slow roll (SR) phase. Our mass bounds are applicable as far as there is no intermediate fast roll stage between the USR and the SR phase. We then extend our formalism to study the imprints of a reheating epoch on both the ISGWB and the derived lower mass bound. We find that a prolonged epoch of a noninstantaneous reheating leads to a shift in the ISGWB energy spectrum towards smaller frequencies. Thus, such an ISGWB signal can be detected simultaneously by different GW observatories. Finally, we study the imprints of a transition from an early matter-dominated (eMD) phase to the RD phase on the ISGWB and find that such a transition leads to a secondary amplification of the ISGWB at a much smaller scale corresponding to the smallest comoving scale leaving the horizon during inflation or the end of the inflation scale.

The remainder of this paper is organized as follows. In the following section, we shall quickly discuss the basic formalism to compute the ISGWB from first-order scalar perturbations in any general inflationary scenario. We shall compute the spectral energy density of GWs today for the scenario of PBH formation of our earlier work and compare it with the optimal (design) sensitivities of various present and future GW observatories. We shall show that the ISGWB induced by ultralight PBHs can be detected by a future run of the ground-based Advanced LIGO detector. In Sec. III, we shall discuss in detail how to obtain the lowest possible PBH mass both for the cases of an instantaneous transition and a smooth transition from the USR to the SR phase. In Sec. IV, we shall study the resulting effects of a noninstantaneous reheating epoch on the GW spectra and the lower bound on the PBH mass as well as a secondary amplification of the ISGWB due to a transition from an eMD phase to the RD phase. Finally, we shall summarize our results and discuss their implications in Sec. V. In the Appendix, we shall provide the details of the calculations of the transition from an eMD to the RD era.

Our conventions and notations adopted in this paper are as follows. We work in the natural units,  $\hbar = c = 1$ , with reduced Planck mass  $M_{\text{Pl}}^2 = (8\pi G)^{-1}$ . The conformal time  $\tau$  is defined as  $d\tau = dt/a(t)$ . The overdots and primes denote the derivatives with respect to the cosmic time  $t$  and the conformal time  $\tau$ , respectively. The Hubble parameter is defined as  $H \equiv \dot{a}/a$  while the conformal Hubble parameter is given by  $\mathcal{H} \equiv aH \equiv a'/a$ .

## II. STOCHASTIC GWs FROM FIRST-ORDER SCALAR PERTURBATIONS

It is well known that, at the linear order in perturbations, the scalar, vector, and tensor perturbations evolve independently (thanks to the decomposition theorem) and that

their evolution is governed by their corresponding equations of motion. However, at the second order in perturbations, an extra source term is generated for the tensor perturbations due to the mode coupling of scalar metric fluctuations which inevitably lead to an ISGWB. In this section, we shall present the basic formalism and essential equations for the tensor perturbations with a source term due to first-order scalar perturbations at quadratic order. We shall then solve these equations numerically for the inflationary scenario of our earlier work [69] and calculate the GW energy density spectrum at the present epoch. We shall also discuss the potential detection of this ISGWB with the future space-based GW observatories such as IPTA, LISA, DECIGO, and Einstein Telescope (ET).

In this section, we shall closely follow the discussion of the seminal paper [49]. Let us start with perturbing the Friedmann-Lemaître-Robertson-Walker metric with the scalar and tensor perturbations. In the conformal Newtonian gauge, the perturbed metric can be written as

$$ds^2 = -a^2(\tau)(1 + 2\Phi)d\tau^2 + a^2(\tau) \left[ (1 - 2\Psi)\delta_{ij} + \frac{1}{2}h_{ij} \right] dx^i dx^j, \quad (2.1)$$

where  $\Phi$  and  $\Psi$  are the scalar metric perturbations, also called the Bardeen potentials, and  $h_{ij}$  is the tensor perturbation which is symmetric ( $h_{ij} = h_{ji}$ ), traceless ( $h_{ii} = 0$ ), and transverse ( $h_{ij,j} = 0$ ). Assuming  $\Phi = \Psi$ , the scalar part of the anisotropic stress (shear) vanishes but the corresponding tensor part does not. As we shall see later, this serves as a source to the evolution equation for tensor perturbations. With the Fourier modes  $h_{\mathbf{k}}$ , the dimensionless power spectrum  $\mathcal{P}_h$  is

$$\frac{k^3}{2\pi^2} \langle h_{\mathbf{k}}^\lambda(\tau) h_{\mathbf{k}'}^{\lambda'}(\tau) \rangle = \delta_{\lambda\lambda'} \delta^3(\mathbf{k} + \mathbf{k}') \mathcal{P}_h(\tau, k), \quad (2.2)$$

where  $\lambda, \lambda' = \{+, \times\}$  represent the two polarizations of tensor perturbations. Now, the GW energy density per logarithmic wavelength can be defined as

$$\Omega_{\text{GW}}(\tau, k) \equiv \frac{1}{\rho_c} \frac{d\rho_{\text{GW}}}{d \ln k} = \frac{\rho_{\text{GW}}(\tau, k)}{\rho_{\text{tot}}(\tau)} = \frac{1}{24} \left( \frac{k}{\mathcal{H}} \right)^2 \overline{\mathcal{P}_h(\tau, k)}, \quad (2.3)$$

where the overline denotes an average over time. The observationally relevant quantity is the energy density  $\Omega_{\text{GW}}$  at the present epoch  $\tau = \tau_0$ . Note that in parity invariant scenarios as in our model, both the polarizations will lead to the same result for the GW spectrum. However, in parity violating situations, the power spectrum will be different for the two polarizations. In particular, when only one helicity mode is exponentially amplified due to dynamical instabilities, the power spectrum turns out to be maximally

helical and has very interesting observational implications. For simplicity, from now on we shall ignore the superscript  $\lambda$  in  $h_{\mathbf{k}}$ .

### A. Induced tensor modes and their power spectrum

Using the standard canonical quantization procedure for  $h_{ij}$ , one finds that the equation of motion for the Fourier modes  $h_{\mathbf{k}}$ , sourced by the scalar perturbations  $\Phi$ , is given by

$$h_{\mathbf{k}}''(\tau) + 2\mathcal{H}h_{\mathbf{k}}'(\tau) + k^2 h_{\mathbf{k}}(\tau) = 4S_{\mathbf{k}}(\tau), \quad (2.4)$$

where  $S_{\mathbf{k}}$  is the Fourier component of the source term comprised of first-order scalar perturbations. This differential equation can be solved by the Green's function method which yields the solution as [55]

$$h_{\mathbf{k}}(\tau) = \frac{4}{a(\tau)} \int^{\tau} d\bar{\tau} a(\bar{\tau}) G_{\mathbf{k}}(\tau, \bar{\tau}) S_{\mathbf{k}}(\bar{\tau}), \quad (2.5)$$

where  $G_{\mathbf{k}}(\tau, \bar{\tau})$  is the solution to the following equation:

$$G_{\mathbf{k}}''(\tau, \bar{\tau}) + \left[ k^2 - \frac{a''(\tau)}{a(\tau)} \right] G_{\mathbf{k}}(\tau, \bar{\tau}) = \delta(\tau - \bar{\tau}). \quad (2.6)$$

Since we are interested in the ISGWB on smaller scales corresponding to  $k \gg k_{\text{eq}}$ , which reenter the horizon during the RD epoch, we shall restrict our following discussion to  $w = 1/3$  only. In the RD universe ( $a \sim \tau$ ), we can express  $G_{\mathbf{k}}(\tau, \bar{\tau})$  as

$$G_{\mathbf{k}}(\tau, \bar{\tau}) = \frac{1}{k} \sin(x - \bar{x}), \quad (2.7)$$

where  $x = k\tau$  and  $\bar{x} = k\bar{\tau}$ , respectively. While  $G_{\mathbf{k}}(\tau, \bar{\tau})$  involves the effects of propagation for the GW, the effects of amplified scalar perturbation come from the source term and depend on the time evolution of the scalar perturbation modes. During the RD era, the ISGWB is produced mainly around the horizon reentry without growing any further, because the gravitational potential oscillates after horizon reentry. At first order, the time evolution of  $\Phi_{\mathbf{k}}$  in RD is governed by

$$\Phi_{\mathbf{k}}''(\tau) + \frac{4}{\tau} \Phi_{\mathbf{k}}'(\tau) + \frac{1}{3} k^2 \Phi_{\mathbf{k}}(\tau) = 0. \quad (2.8)$$

We can split  $\Phi_{\mathbf{k}}(\tau)$  into a primordial part,  $\tilde{\Phi}_{\mathbf{k}}$  (the value at the start of RD), and the transfer function,  $\mathcal{T}(k\tau)$ , representing the time evolution as  $\Phi_{\mathbf{k}}(\tau) = \mathcal{T}(k\tau) \tilde{\Phi}_{\mathbf{k}}$ . Note that, in the RD era, the scalar perturbation  $\Phi_{\mathbf{k}}$  is directly related to the gauge invariant comoving curvature perturbation by  $\tilde{\Phi}_{\mathbf{k}} = \frac{2}{3} \mathcal{R}(\mathbf{k})$ . The full solution for Eq. (2.8) for  $\mathcal{T}(k\tau)$  can be found in the Appendix. For an instantaneous reheating history, we assume for  $\tau \rightarrow 0$  that  $\mathcal{T}(k\tau) \rightarrow 1$  and

$\mathcal{T}'(k\tau) \rightarrow 0$ , and we can express  $\mathcal{T}(k\tau)$  as a function of  $x$  by

$$\mathcal{T}(x) = \frac{9}{x^2} \left[ \frac{\sqrt{3}}{x} \sin\left(\frac{x}{\sqrt{3}}\right) - \cos\left(\frac{x}{\sqrt{3}}\right) \right]. \quad (2.9)$$

One can find the detailed calculation of the induced tensor spectrum in [55,58,79] and thus, we shall directly write the final expression of the second-order tensor power spectra.

The calculation of the tensor power spectrum  $\mathcal{P}_h$  will involve the four point functions of  $\mathcal{R}(\mathbf{k})$ . However, we can assume it to be Gaussian at leading order and use Wick's theorem to write the four point functions in terms of possible combinations of the two point functions or the power spectrum  $\mathcal{P}_{\mathcal{R}}(k)$ . After a lot of simplification, one finds

$$\mathcal{P}_h(\tau, k) = 4 \int_0^\infty dv \int_{|1-v|}^{1+v} du \left( \frac{4v^2 - (1+v^2 - u^2)^2}{4uv} \right)^2 \times I_{\text{RD}}^2(v, u, x) \mathcal{P}_{\mathcal{R}}(kv) \mathcal{P}_{\mathcal{R}}(ku), \quad (2.10)$$

where  $v = p/k$ ,  $u = |\mathbf{k} - \mathbf{p}|/k$ , and the factor  $I_{\text{RD}}$  is defined as

$$I_{\text{RD}}(u, v, x) = \int_{x_r}^x d\bar{x} \frac{\bar{x}}{x} f(u, v, \bar{x}, x_r) kG(\bar{x}, x), \quad (2.11)$$

where  $x_r = k\tau_r$  corresponds to the conformal time  $\tau_r$  at the beginning of RD phase, and  $x = k\tau$  corresponds to some late time  $\tau$  during the RD epoch. For instantaneous reheating, we can take  $x_r \rightarrow 0$ . The factor  $I(u, v, x)$  is a very involved function and we have derived its general

form for the RD universe preceded by an eMD era in the Appendix, from which the results for the instantaneous reheating case can be recovered by taking the appropriate limit  $x_r \rightarrow 0$ .

To calculate the present energy density of the ISGWB, we can evolve the integration  $I(u, v, x)$  up to a time when standard model degrees of freedom become nonrelativistic and find  $\Omega_{\text{GW}}(\tau, k)$ . Using the entropy conservation, we can then express the present ISGWB energy density,  $\Omega_{\text{GW}}(\tau_0, k)$ , in terms of present radiation energy density,  $\Omega_{r,0}$ ,  $\Omega_{\text{GW}}(\tau, k)$ , and a constant  $c_g$  as [79]

$$\begin{aligned} \Omega_{\text{GW}}(\tau_0, k) &= c_g \Omega_{r,0} \Omega_{\text{GW}}(\tau, k) \\ &= \frac{1}{24} \left( \frac{k}{\mathcal{H}} \right)^2 c_g \Omega_{r,0} \overline{\mathcal{P}_h(\tau, k)}, \end{aligned} \quad (2.12)$$

where  $c_g \approx 0.4$  if we take the number of relativistic degrees of freedom to be  $\sim 106$ . In the RD epoch,  $\mathcal{H} = aH = 1/\tau$ , and we can write  $k/\mathcal{H} = k\tau = x$ , so taking the  $k/\mathcal{H}$  factor inside the power spectra integral and defining  $\mathcal{I}$  with  $I = \mathcal{I}/x$ , we can write

$$\begin{aligned} \Omega_{\text{GW}}(\tau_0, k) &= \frac{1}{6} c_g \Omega_{r,0} \int_0^\infty dv \\ &\times \int_{|1-v|}^{1+v} du \left( \frac{4v^2 - (1+v^2 - u^2)^2}{4uv} \right)^2 \\ &\times \bar{\mathcal{I}}_{\text{RD}}^2(v, u, x) \mathcal{P}_{\mathcal{R}}(kv) \mathcal{P}_{\mathcal{R}}(ku). \end{aligned} \quad (2.13)$$

In the late time limit  $x \rightarrow \infty$  for a pure RD universe one gets

$$\begin{aligned} \bar{\mathcal{I}}_{\text{RD}}^2(v, u, x \rightarrow \infty) &= \frac{1}{2} \left( \frac{3(u^2 + v^2 - 3)}{4u^3 v^3} \right)^2 \left[ \left( -4uv + (u^2 + v^2 - 3) \log \left| \frac{3 - (u+v)^2}{3 - (u-v)^2} \right| \right)^2 \right. \\ &\left. + \pi^2 (u^2 + v^2 - 3)^2 \Theta(u + v - \sqrt{3}) \right]. \end{aligned} \quad (2.14)$$

Note that while this formula is valid for an instantaneous reheating history, a more general expression for  $\bar{\mathcal{I}}_{\text{RD}}^2$ , assuming the RD phase is preceded by an eMD phase, is derived in the Appendix.

In our previous work [69], we had developed a numerical code to compute the PBH mass fraction for inflationary models which allows violations of the SR condition needed for the enhancement of the power spectrum. We have chosen a different set of parameters for our model in such a way that the largest possible mass fraction of the PBHs is obtained as allowed by various constraints in a given mass range. We have now extended that code by including a routine to compute the ISGWB in such models. In Fig. 1 (on the left), we have plotted the power spectra of

primordial curvature and tensor perturbations  $\mathcal{P}_{\mathcal{R}}$  and  $\mathcal{P}_h$  for the scenario that we had discussed in our earlier work [69]. The power spectra  $\mathcal{P}_{\mathcal{R}}$  correspond to different choices of parameters of the model which leads to different values of the spectral index  $n_s$  at the pivot scale. All these spectra show a similar enhancement,  $\mathcal{P}_{\mathcal{R}} \sim k^4$ , at smaller scales, an interesting behavior which has also been obtained using an analytical formalism [80,81]. The spectral distortion constraints on the primordial power spectrum derived from COBE/FIRAS and forecasts for PIXIE are also shown [82]. It is well known that the amplitude of the power spectrum of curvature perturbations should be  $P_{\mathcal{R}} \sim 10^{-2}$  to form PBHs in radiation domination. Assuming a specific functional form of the scalar spectrum, one can

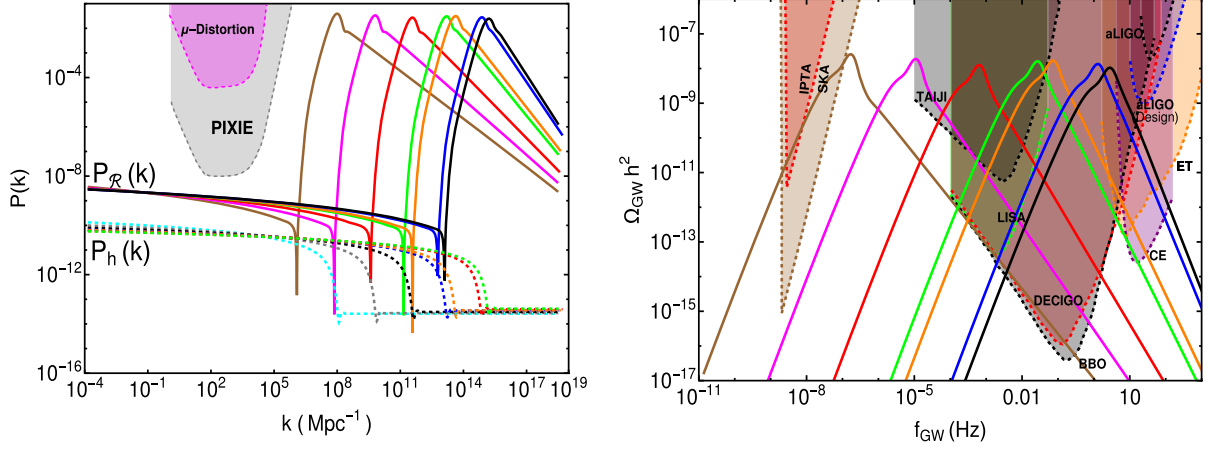


FIG. 1. On the left, we plot the power spectra of primordial curvature perturbations  $\mathcal{P}_{\mathcal{R}}$  (solid curves) and primordial tensor perturbations  $\mathcal{P}_h$  (dashed curves) for different parameters of the scenario proposed in our earlier work [69]. All these spectra show a similar enhancement at smaller scales, required for the abundant PBH production. Also shown are the relevant constraints from cosmic microwave background (CMB) spectral distortions [82,84]. On the right, we plot the spectral energy density of the ISGWB corresponding to the spectra on the left. All the GW spectra also show similar behavior. In particular, a bump in  $\mathcal{P}_{\mathcal{R}}$  on small scales leads to a peak in  $\Omega_{\text{GW}} h^2$  on larger frequencies which fall in the sensitivity regimes of various future space-based GW observatories such as IPTA, LISA, DECIGO, and ET. The color coding of different plots is consistent across the two figures.

arrive at a rough order of magnitude estimation of the PBH nondetection constraints, as shown in [80]. However, this estimate also depends upon the shape of the power spectrum, as has already been shown in [83]. It further depends on the choice of the critical density contrast, the window function, the collapse formalism, etc., as discussed in Appendix B of our earlier paper [69]. Unless one obtains these PBH constraints for the specific model of interest, it is not appropriate to use them for comparison with another model. For this reason, we are not displaying such constraints in our plots in Fig. 1. Moreover, to facilitate easy comparison, we are following the same color coding as in Fig. 3 of our previous paper [69].

In the right panel of Fig. 1, we have plotted the corresponding spectral energy density of induced GWs,  $\Omega_{\text{GW}} h^2$ , obtained by numerically integrating Eq. (2.13). We found that all the GW spectra show similar behavior, with a peak at a characteristic frequency determined by the relation (2.16). As expected, a bump in  $\mathcal{P}_{\mathcal{R}}$  leads to a peak in  $\Omega_{\text{GW}} h^2$ , which fall in the sensitivity regimes of various future space-based GW observatories such as IPTA, LISA, DECIGO, and ET. As we have found in our scenario, a wider power spectrum  $\mathcal{P}_{\mathcal{R}}$  will result in a wider induced GW spectra spanning a broader frequency range. This is interesting because the induced signal overlaps with the design sensitivity plots of different upcoming GW observatories, particularly around the mHz–Hz range. In such a situation, there lies an interesting possibility to simultaneously detect these signals with different observatories and obtain stronger constraints on its origins in terms of the model parameters. It is also interesting to note that for some cases in our model, wherein the bump in the scalar power spectrum is located on rather larger scales (but still much

smaller than CMB scales), the resulting induced GW background can also be detected by an array of future IPTA/SKA detectors [85,86]. Future observations of CMB spectral distortions will also strongly constrain the primordial power spectrum in the regime  $1 \text{ Mpc}^{-1} \lesssim k \lesssim 10^5 \text{ Mpc}^{-1}$  [84,87].

## B. Observing ultralight PBHs with Advanced LIGO

As we had mentioned in our earlier work [69], our scenario can produce PBHs in very different mass ranges and all these mass windows are constrained by a variety of observations. However, it turns out that there does not seem to be any observational constraints around the asteroid mass window and thus, PBHs could contribute to the total energy density of CDM around that window, as has been emphasized in the literature recently. It is well known that PBHs do evaporate due to Hawking radiation and that the evaporation time scale is given by

$$t_{\text{ev}}(M) \sim \frac{G^2 M^3}{\hbar c^4} \sim 10^{63} \left( \frac{M}{M_{\odot}} \right)^3 \text{ yr}. \quad (2.15)$$

This implies that PBHs with mass  $M \lesssim 10^{-18} M_{\odot}$  ( $M \lesssim 10^{15} \text{ g}$ ) would be completely evaporated by today and thus can not contribute to the present density of the CDM in the universe [88,89]. PBHs in the mass range  $10^{-18} - 10^{-16} M_{\odot}$  would actually be evaporating at the present epoch and thus can induce an observable  $\gamma$ -ray background [90]. However, PBHs in the very low mass range would not contribute to the CDM at all and would also be completely evaporated by today. However, they might still induce a secondary GW background which

could, in principle, be detected by the future designs of the ground-based GW observatories.

It is interesting to note that the three ‘‘peaks,’’ i.e., the position of the peak in the power spectrum of curvature perturbations, the peak height in the PBH mass distribution, and the frequency of the peak of the GW signal, are related by [54,57,91]

$$\left(\frac{M_{\text{PBH}}}{10^{17} \text{ g}}\right)^{-1/2} \simeq \frac{k}{2 \times 10^{14} \text{ Mpc}^{-1}} = \frac{f}{0.3 \text{ Hz}}, \quad (2.16)$$

which provides a qualitative understanding of the relation among  $M_{\text{PBH}}$ ,  $k$ , and  $f$ . This relation roughly indicates that a peak in the power spectrum of curvature perturbations at  $k \simeq 2 \times 10^{14} \text{ Mpc}^{-1}$  would generate a peak in the GW spectrum at frequency  $f \sim 0.3 \text{ Hz}$ . Moreover, as the sensitivity is maximum for LISA at  $f \sim \text{mHz}$ , the peak in  $\mathcal{P}_{\mathcal{R}}$  should be around  $k \sim 10^{12} \text{ Mpc}^{-1}$ , which is consistent with what is shown in Fig. 1. This scaling can further be used to roughly figure out what mass range of PBHs can possibly be probed by means of their secondary GW signatures using the ground-based detectors such as Advanced LIGO. The maximal sensitivity of the projected design of the Advanced LIGO detector corresponds to  $f \sim 30 \text{ Hz}$ . A stochastic GW signal around this frequency would correspond to very light PBHs with mass around  $M_{\text{PBH}} \sim 10^{13} \text{ g} \sim 10^{-20} M_{\odot}$ . Evidently, from Eq. (2.15), all such PBHs would be completely evaporated through the emission of Hawking radiation from their formation to today and thus can not constitute the observed abundance of CDM.

Note that  $M_{\text{PBH}}$  here corresponds to the mass of a PBH at the formation epoch and disregards any further mass growth due to merging or accretion. Moreover, there exists various uncertainties associated with the numbers in this equation, e.g., the efficiency factor  $\gamma$  which is defined as the ratio between the mass collapsing into a PBH and the total mass associated to that mode within the horizon. Its value is usually taken as  $\gamma \sim 0.2$  [88,92] but there could be some uncertainties associated with the PBH collapse. Often, the effects of the critical collapse are neglected wherein detailed numerical work has shown that the mass of PBHs formed after horizon reentry will depend on the amplitude of the overdensity  $\delta$ . Secondly, a slightly smaller value of the radiation energy density today will lead to an  $\mathcal{O}(1)$  difference in this relation. Finally, a slight difference arises due to the value of  $g_*$ , the relativistic number of degrees of freedom in the thermal bath when the mode responsible for the PBH reenters the horizon, although the dependence of  $M_{\text{PBH}}$  on  $g_*$  is weak. All these uncertainties could introduce a factor of  $\mathcal{O}(10)$  in the final result so one should keep them in mind when comparing this relation with an exact numerical calculation, as is the case with our scenario.

In Fig. 2, we have plotted the PBH mass fractions at the formation epoch  $\beta_{\text{ini}}$  and the associated secondary GW

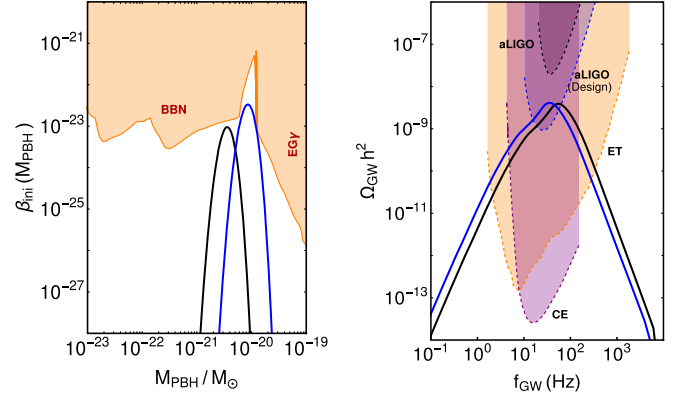


FIG. 2. On the left, we plot the initial PBH mass fraction  $\beta_{\text{ini}}$  (at formation) for two different cases, produced in our model [69] in the very low mass range corresponding to  $M \sim 10^{-20} - 10^{-21} M_{\odot}$ , as well as the observational constraints arising from BBN and the extragalactic  $\gamma$ -ray background. Note that while comparing the constraints on  $\beta_{\text{ini}}$ , we are assuming the mass fractions of our model to be monochromatic. Such small-mass PBHs would have been completely evaporated by today due to Hawking radiation. However, they will still induce an observable ISGWB in the higher frequency range which falls in the design sensitivity contours of the Advanced LIGO detector and therefore can, in principle, be detected in future runs, as shown on the right.

energy densities for two different cases of our scenario [69]. Since the PBH mass fraction at matter-radiation equality  $\beta_{\text{eq}}$  can be expressed as  $\beta_{\text{eq}} \simeq (a_{\text{eq}}/a_{\text{ini}})\beta_{\text{ini}}$ , this implies that  $\beta_{\text{eq}}$  can be quite large even for a very small  $\beta_{\text{ini}}$ . Since low mass PBHs will evaporate very quickly,  $\beta_{\text{ini}}$  is the only relevant quantity for such PBHs and thus, we have optimized our parameters<sup>1</sup> such that we obtain  $\beta_{\text{ini}} \sim 10^{-23}$ , as allowed by the constraints arising from the big bang nucleosynthesis (BBN) and the extragalactic  $\gamma$ -ray background. However, as pointed out recently in [36] and as we also observed in our inflationary model, their ISGWB falls right in the design sensitivity curves of a future configuration of the Advanced LIGO detector and thus can potentially be detected. Moreover, this ISGWB also falls in the sensitivity contours of the proposed third-generation ground-based GW detectors, the ET and Cosmic Explorer (CE). Since this ISGWB overlaps with these three future GW detectors, there lies again an interesting possibility of its simultaneous detection with these GW observatories and thereby putting stronger constraints on its origin. Note that the ground-based GW detectors such as LIGO and VIRGO have already detected the astrophysical GW signals from a few systems of binary black holes and neutron stars with large masses and will detect many more in the near future.

<sup>1</sup>In order to obtain an appropriate fraction of initial PBH abundance, we need to fine-tune the potential parameters, following the same method as in [69], which requires slight deviations from the exact inflection point conditions of the inflationary potential.

However, the characteristic shapes of the GW spectrum in these two cases are very different and thus can be easily disentangled. Recently, some prospects of probing such ultralight PBHs using their ISGBW signatures with the Advanced LIGO detector have been discussed in [93].

### III. A LOWER BOUND ON THE PBH MASSES FOR USR INFLATION

In this section, we shall discuss how to obtain a stringent lower bound on the PBH masses in the USR phase, both using an instantaneous transition as well as a smooth transition from the USR to the SR phase. We find that the lower bound obtained in both of the scenarios are in agreement with each other. Moreover, our bounds also effectively apply even if there are brief deviations from the SR phase after the USR phase.

#### A. An instantaneous transition from USR to SR

In order to estimate the lower bound, we first need an estimation of the minimum number of  $e$ -folds in the final SR phase followed by the USR phase. Assuming that the inflaton is rolling in the positive direction,  $\phi_N = d\phi/dN$  is positive. Since  $\phi_N$  always decreases during the USR phase, let's assume that at  $N = N_0$ ,  $\phi_N$  reaches its minimum value. This can also be considered the point after which the SR potential takes over and  $\phi_N$  starts to increase again. Note that, at this point,  $\phi_{NN} = 0$  and as the first SR parameter,  $\epsilon = \phi_N^2/2M_{\text{Pl}}^2$ , is very small, the second SR parameter,  $\eta = \epsilon - (\phi_{NN}/\phi_N)$ , is also very small and as a result, all the SR conditions are satisfied. Thus we can safely approximate the power spectrum of  $\mathcal{R}_k$  with the SR result as

$$P_{\mathcal{R}}(k) \simeq \frac{1}{8\pi^2 M_{\text{Pl}}^2} \frac{H^2}{\epsilon_0}, \quad (3.1)$$

where  $\epsilon_0 = \epsilon(N_0)$ . Since we are considering an instantaneous transition from the USR to the SR phase, the smallest scale  $k_0 = k(N_0)$  leaving the horizon would still be amplified and produce PBHs. Moreover, a significant mass fraction of PBHs requires an amplification of the power spectrum at PBH scales as  $P_{\mathcal{R}}(k) \sim 10^{-2}$ , so Eq. (3.1) leads to

$$\epsilon_0 \simeq \frac{H^2}{M_{\text{Pl}}^2}. \quad (3.2)$$

Now, using the SR approximation during the horizon exit of the observable pivot scale  $k_p$ , we can safely use Eq. (3.1) to estimate the Hubble parameter,  $H$ , which stays nearly constant during inflation as

$$\frac{H^2}{M_{\text{Pl}}^2} \sim 10^{-9}, \quad (3.3)$$

where we have used  $P_{\mathcal{R}}(k_p) \sim 2.1 \times 10^{-9}$  and  $\epsilon_p \sim 10^{-2}$  using  $n_s(k_p) \simeq 0.965$ . Now using (3.2) and (3.3), we can estimate the minimum value of  $\epsilon_0$  as  $\epsilon_0 \sim 10^{-9}$  and the corresponding minimum value of  $|\phi_{N_0}| \simeq \sqrt{2} \times 10^{-4.5}$ . Using this estimation, we want to understand the minimum number of  $e$ -folds necessary from  $N = N_0$  to the end of inflation at  $N = N_e$ , where  $\epsilon(N_e) = 1$  or  $\phi_{N_e} = \sqrt{2}$  must be satisfied. For this calculation, we shall assume that SR conditions are not violated again between the end of the USR phase and the end of inflation, and thus, the two conditions must be satisfied,  $\epsilon \ll 1$  and  $|\eta| \leq 1$ . This leads to the following inequality:

$$-1 \leq \frac{\phi_{NN}}{\phi_N} \leq 1 \quad \text{or} \quad \left| \frac{\phi_{NN}}{\phi_N} \right| \leq 1. \quad (3.4)$$

If we assume  $\phi_{NN}/\phi_N = c(N)$ , and solve it with the initial condition  $\phi_N(N = N_0) = \phi_{N_0}$ , we obtain

$$\log \left| \frac{\phi_N}{\phi_{N_0}} \right| = \int_{N_0}^{N_e} c(N) dN. \quad (3.5)$$

Now using (3.4),  $|c(N)| \leq 1$ , so the minimum number of  $e$ -folds between  $N_0$  and the end of inflation  $N_e$  ( $\phi_{N_e} = \sqrt{2}$ ) is constrained as

$$\Delta N = N_e - N_0 \geq \log \left| \frac{\sqrt{2}}{\phi_{N_0}} \right|. \quad (3.6)$$

Using our previous estimation,  $|\phi_{N_0}| \simeq \sqrt{2} \times 10^{-4.5}$ , we get  $\Delta N \geq 10.36$ , which is roughly the duration of the final SR phase before the end of inflation.

#### B. A smooth transition from USR to SR

Our previous estimation of the minimum number of  $e$ -folds was independent of the form of the potential and we only assumed an instantaneous transition from the USR to SR phase. To extend our analysis for a smooth transition from USR to SR, we need to consider the potential around  $\phi(N_0) \equiv \phi_0$ . Since the USR phase is on a flat part of the potential, we can effectively approximate the potential around  $\phi_0$ , with the first few terms of the Taylor's expansion as

$$V(\phi) = b_0 + b_1(\phi - \phi_0) + b_2(\phi - \phi_0)^2 + \dots \quad (3.7)$$

In the vicinity of the USR phase, we can neglect the  $\phi_N^2$  term and assume the Hubble parameter to be constant as  $H(N) \simeq \sqrt{V(\phi_0)/3} = \sqrt{b_0/3}$ . This reduces the equation of motion for  $\phi$  to

$$\phi_{NN} + 3\phi_N + \frac{1}{H^2} \frac{dV}{d\phi} = 0. \quad (3.8)$$

Now, using the initial condition that at  $N = N_0$  the inflation field value is  $\phi_0$  and the minima of  $\phi_N$  is reached, i.e.,  $\phi_{NN} = 0$ , we obtain the dynamics of  $\phi$  as [94]

$$\begin{aligned} \phi(N) &= \phi_0 - \frac{b_1}{2b_2} + \frac{1}{4\alpha b_2} \\ &\times \left[ \left( \alpha b_1 + \frac{4b_1 b_2}{3H} - 3b_1 H \right) e^{-\frac{(\alpha+3H)(N-N_0)}{2H}} \right. \\ &\left. + \left( \alpha b_1 + \frac{4b_1 b_2}{3H} - 3b_1 H \right) e^{\frac{(\alpha-3H)(N-N_0)}{2H}} \right], \end{aligned}$$

where  $\alpha = \sqrt{3b_0 - 8b_2}$ . Assuming that the inflaton is rolling in the positive direction, at the minima  $\phi_N$  must be positive to have a finite duration of the USR phase. Thus, we need

$$\phi_N(N_0) = -\frac{b_1}{b_0} > 0 \quad \text{and} \quad \phi_{NNN}(N_0) = \frac{(6b_1 b_2)}{b_0^2} > 0. \quad (3.9)$$

These conditions constrain the possible value of the potential parameters  $b_1 < 0$  and  $b_2 < 0$ . Using these, we can now express  $\phi_N$  as a function of a single positive parameter  $b_6$  as

$$\begin{aligned} \frac{\phi_N(N)}{\phi_N(N_0)} &= \frac{\sqrt{3}}{b_6} e^{-3\Delta N/2} \sinh\left(\frac{\sqrt{3}}{2} b_6 \Delta N\right) \\ &+ e^{-3\Delta N/2} \cosh\left(\frac{\sqrt{3}}{2} b_6 \Delta N\right), \end{aligned} \quad (3.10)$$

where  $b_6 = \sqrt{3b_0 - 8b_2}/\sqrt{b_0}$  and  $\Delta N = N - N_0$ . To avoid eternal inflation, we need  $b_2 < 0$ , so the minimum value of  $b_6$  must be greater than  $\sqrt{3}$ . Now we want to estimate the number of  $e$ -folds from the peak in the power spectra to the point where the SR potential takes over completely (let's say at  $N = N_s$ ). Our assumption is that this transition to the SR phase must happen while  $|\eta| \leq 1$ , which then leads to

$$\epsilon(\Delta N) = 10^{-9} \left( \frac{\phi_N(\Delta N)}{\phi_N(N_0)} \right)^2, \quad (3.11)$$

$$\begin{aligned} \eta(\Delta N) &= \epsilon(\Delta N) - \frac{\phi_{NN}(\Delta N)}{\phi_N(\Delta N)} \\ &= \epsilon(\Delta N) + \frac{9 - 3b_6^2}{2\sqrt{3}b_6 \coth\left(\frac{\sqrt{3}}{2} b_6 \Delta N\right) + 6}. \end{aligned} \quad (3.12)$$

When the minima of  $\phi_N$  is reached,  $\phi_{NN} = 0$ ,  $\epsilon$  is very small ( $\epsilon \sim 10^{-9}$ ), and thus around  $N = N_0$ ,  $\eta$  crosses zero. Just after this crossing,  $\phi_{NN}$  starts to increase and achieves a positive value, which leads to an increase in  $\phi_N$  as well. Very quickly, the ratio  $\phi_{NN}/\phi_N$  saturates, which is the second term of  $\eta$  with a negative sign, as in (3.12). It is

interesting to note that depending on the value of  $b_6$ , this term saturates to a negative asymptotic value  $\eta_{\text{asym}} = \frac{9-3b_6^2}{2\sqrt{3}b_6+6}$ . Evidently, this saturation indicates the end of the transition phase. After this point, the further dynamics must be completely described by the SR potential. If this saturation value  $\eta_{\text{asym}} \leq -1$ , the dynamics deviate from the SR phase before the transition and enter a fast roll phase. We shall assume that there is no intermediate fast roll phase between USR and SR and consider only values of  $b_6$  which ensure the transition to SR before  $\eta \simeq -1$ . Thus, solving for  $\phi_{NN}/\phi_N = 1$ , we obtain

$$N(b_6) = \frac{2}{\sqrt{3}b_6} \coth^{-1}\left(\frac{\sqrt{3}(b_6^2 - 5)}{2b_6}\right). \quad (3.13)$$

In our case,  $b_6$  is already constrained as  $b_6 > \sqrt{3}$ . The above equation further limits the value of  $b_6$  to be less than  $5/\sqrt{3}$  so we finally have  $\sqrt{3} < b_6 \leq 5/\sqrt{3}$ .

Now we want to understand what can be the maximum value of  $\epsilon_s$  or  $\phi_{N_s}$  during this transition and how many  $e$ -folds are spent to reach the transition. If we solve  $\eta = -c$  for  $0 < c < 1$ , from (3.12) we get

$$N_c(b_6) = \frac{2}{\sqrt{3}b_6} \coth^{-1}\left(\frac{\sqrt{3}(b_6^2 - 2c - 3)}{2b_6 c}\right). \quad (3.14)$$

Upon using (3.14), at  $N = N_c$  we can find  $\epsilon$  as a function of  $b_6$  as

$$\begin{aligned} \epsilon(b_6) &= 3 \times 10^{-9} \frac{(b_6^2 - 3)}{3b_6^2 - (2c + 3)^2} \\ &\times \exp\left[-\frac{2\sqrt{3}}{b_6} \coth^{-1}\left(\frac{\sqrt{3}(b_6^2 - 2c - 3)}{2b_6 c}\right)\right]. \end{aligned} \quad (3.15)$$

This value of  $\epsilon$  is plotted in Fig. 3 (on the left) and from this plot we can clearly see that for every  $b_6$  in the range  $\sqrt{3} < b_6 \leq 5/\sqrt{3}$ ,  $\eta$  saturates to a constant value,  $\eta > -1$ . We can consider this saturation to be the beginning of the SR phase and we need to use the value of  $\epsilon$  during this saturation as the starting value of  $\epsilon_s$  for the SR phase. Solving for  $\phi_{NN}/\phi_N = -\eta_{\text{asym}} + \xi$ , where  $\xi$  is negative and much smaller than  $\eta_{\text{asym}}$ , we can get the value of the  $e$ -fold number where  $\eta$  reaches its asymptotic value and the value of  $\epsilon_s$ , as plotted on the right in Fig. 3. It is evident from these plots that  $b_6 = 5/\sqrt{3}$  leads to the highest value of  $\epsilon_s \simeq 7.0 \times 10^{-8}$  and the lowest value of  $N_s - N_0 \simeq 2.34721$ . This also corresponds to the quickest transition and the largest possible transition value of  $|\eta_s|$ , whereas  $b_6 \rightarrow \sqrt{3}$  leads to the lowest value of  $\epsilon_s \simeq 1.0 \times 10^{-9}$  and the largest value of  $N_s - N_0 \simeq 3.83$ .

Finally, the above values of  $\epsilon_s$  can be translated to the bound on the number of  $e$ -folds using (3.6), and thus we

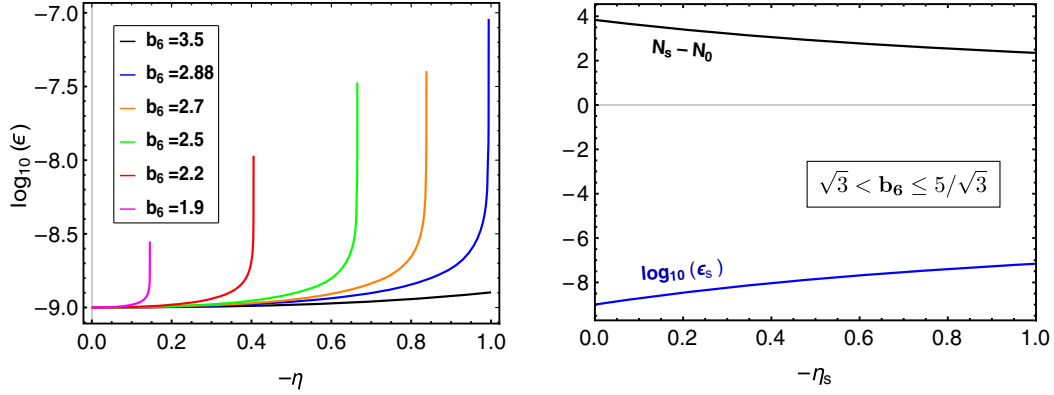


FIG. 3. On the left, we have plotted the growing behavior of  $\epsilon$  before the transition, as obtained in Eq. (3.15). It is evident that for all values of  $b_6$  in the range  $\sqrt{3} < b_6 \leq 5/\sqrt{3}$ ,  $\eta$  saturates to a constant value greater than  $-1$ . On the right is the largest value of  $\epsilon_s$  and the corresponding number of  $e$ -folds whenever  $\eta$  reaches its asymptotic value  $\eta_s$ .

can calculate the total number of  $e$ -folds, before and after the SR transition for both the cases, as

- (1) For  $b_6 = 5/\sqrt{3}$ ,  $\Delta N_{\min} \simeq 2.35 + 8.23 = 10.58$ ,
- (2) For  $b_6 \rightarrow \sqrt{3}$ ,  $\Delta N_{\min} \simeq 3.83 + 10.36 = 14.19$ .

Thus, it is evident that for a smooth transition, even the quickest possible transition takes more numbers of  $e$ -folds than our estimation in the previous section wherein we considered an instantaneous transition in a rather model-independent manner.

### C. Estimation of the lower bound on the PBH mass

In order to estimate a lower bound on the PBH mass from the USR phase, we first need to calculate the total number of  $e$ -folds from the horizon exit of the pivot scale  $k_p = 0.05 \text{ Mpc}^{-1}$  to the end of inflation. In the RD universe,  $a \propto t^{1/2}$ ,  $H \propto t^{-1}$ , and  $k = aH \propto t^{-1/2} \propto H^{1/2}$ . Thus if a comoving wavenumber  $k$  reenters the horizon during the RD epoch, we can relate it with the comoving mode  $k_{\text{eq}}$  of matter-radiation equality using the Hubble parameter during reentry as

$$\frac{k}{k_{\text{eq}}} = \left( \frac{H}{H_{\text{eq}}} \right)^{1/2}. \quad (3.16)$$

Upon using  $\rho_{\text{eq}} = 3H_{\text{eq}}^2 M_{\text{Pl}}^2$ ,  $H_{\text{eq}}$  can be related to the present Hubble parameter as

$$\rho_{\text{eq}} = 2\Omega_{r,0}\rho_c(1+z_{\text{eq}})^4 = 6\Omega_{r,0}H_0^2 M_{\text{Pl}}^2(1+z_{\text{eq}})^4, \quad (3.17)$$

$$H_{\text{eq}} \simeq \sqrt{\Omega_{r,0}}H_0(1+z_{\text{eq}})^2. \quad (3.18)$$

Taking  $\Omega_{r,0} \simeq 8 \times 10^{-5}$ ,  $z_{\text{eq}} \simeq 3400$ , and  $H_0 \simeq 2 \times 10^{-4} \text{ Mpc}^{-1}$ , we find  $H_{\text{eq}} \simeq 20.7 \text{ Mpc}^{-1}$ . Note that we are calculating  $H_{\text{eq}}$  by only taking into account the radiation energy density at the matter-radiation equality. Now at the pivot scale, we know both the amplitude and the tilt of the primordial spectrum from Planck, so using (3.1), we can calculate  $H_{\text{inf}}$  during

inflation which we assume to stay nearly constant up to the end of inflation, which, for instantaneous reheating, is the same as with the beginning of the RD epoch. So  $H_{\text{inf}} \simeq H_e \simeq H_r$ , which is given by

$$H_e \simeq H_r \simeq (8\pi^2 M_{\text{Pl}}^2 P_{\mathcal{R}}(k)\epsilon)^{1/2}. \quad (3.19)$$

With this and (3.16), we can now calculate the comoving mode entering at the very beginning of the RD epoch,  $k_r = a_r H_r$ , as

$$k_r \simeq \frac{k_{\text{eq}}}{\sqrt{H_{\text{eq}}}} (8\pi^2 M_{\text{Pl}}^2 P_{\mathcal{R}}(k)\epsilon)^{1/4}. \quad (3.20)$$

Taking  $k_{\text{eq}} \simeq 0.01 \text{ Mpc}^{-1}$  and  $P_{\mathcal{R}}(k) \simeq 2.1 \times 10^{-9}$  at  $k = k_p$ , we find

$$k_r \simeq 1.94 \times 10^{24} \epsilon^{1/4} \text{ Mpc}^{-1}. \quad (3.21)$$

For the case of an instantaneous reheating, we can finally estimate the total number of  $e$ -folds from the horizon exit of the pivot scale to the end of inflation:

$$N_e - N_p = \ln\left(\frac{k_r}{k_p}\right) \simeq 58.92 + \frac{1}{4} \ln \epsilon. \quad (3.22)$$

Using observational constraints on the value of  $n_s \simeq 0.965$  at the pivot scale, we can roughly estimate  $\epsilon \leq 10^{-2}$ , which then limits  $N_e - N_p \lesssim 57.77$ . This is, of course, consistent with the results from [95] wherein the total number of  $e$ -folds from the horizon exit of the present horizon ( $k_{\text{hor}} \simeq 2 \times 10^{-4} \text{ Mpc}^{-1}$ ) to the end of inflation is constrained to be  $\Delta N_{\text{tot}} \simeq 63.3$ .

We now want to estimate the maximum number of  $e$ -folds from the horizon crossing of  $k_p$  to the minima of  $\phi_N$  at  $N = N_0$ , which we can translate to the smallest scale becoming super-horizon before the onset of the final SR

phase. Assuming the Hubble parameter  $H$  to be nearly constant and  $k_p = a(N_p)H = a_i e^{N_p} H$ , where  $a_i$  is the scale factor at the beginning of inflation, using (3.6) and (3.22) we get

$$N_0 - N_p \simeq 57.77 - 10.36 = 47.41. \quad (3.23)$$

This corresponds to a scale  $k_{\text{PBH}} = \sigma a(N_0)H$ , which becomes super-horizon around  $N = N_0$ . Here,  $\sigma \ll 1$  is taken to ensure that the super-horizon condition is satisfied:

$$k_{\text{max}} = \sigma k_p e^{N_0 - N_p} \approx 1.94 \times 10^{19} \sigma \text{ Mpc}^{-1}. \quad (3.24)$$

Thus the smallest possible comoving-length scale associated with a PBH peak corresponds to  $k_{\text{max}}$ , or  $k_{\text{PBH}} \leq k_{\text{max}}$ . Now we can use the relation between the mass of PBHs and the frequency of second-order induced GWs as in Eq. (2.16) to translate the upper limit on  $k$  in the above equation to a lower limit on the PBH mass,  $M_{\text{PBH}}$  and an upper limit on the frequency of corresponding second-order GWs,  $f$ , as

$$M_{\text{PBH}} \geq 6.14 \times 10^{-27} \sigma^{-2} M_{\odot}, \quad (3.25)$$

$$f \leq 2.91 \times 10^4 \sigma \text{ Hz}. \quad (3.26)$$

Now, if we take a very conservative limit on the factor  $\sigma$  as  $\sigma \leq 10^{-2}$ , the lowest possible value of PBH mass and the highest value of the second-order GW frequency turn out to be  $M_{\text{PBH}} \geq 6.14 \times 10^{-23} M_{\odot}$  and  $f \leq 2.91 \times 10^2 \text{ Hz}$ , respectively. Interestingly, these constraints just cover the Advanced LIGO frequency range so future runs of Advanced LIGO can be used to detect the existence of PBHs from USR models, as we have already discussed in detail in Sec. II B.

Recently, it has also been discussed in the literature that during their formation, the abundance of PBHs with masses  $M < 10^9 \text{ g} \sim 5 \times 10^{-25} M_{\odot}$  are essentially not constrained so they can constitute the dominant component of energy density (since they behave as matter) and drive the dynamics of the universe for a brief period of time before their evaporation due to Hawking radiation [96]. However, our analysis and results of these sections suggest that the USR models of inflation can not possibly produce such ultra low mass PBHs to dominate the energy density of the universe for even a short period of time. Thus one has to resort to a different mechanism of PBH production to discuss those possibilities. It may be interesting to see if an intermediate fast roll phase can produce such ultra low mass PBHs which can dominate for a short while before their evaporation.

## IV. IMPRINTS OF REHEATING ON THE LOWER MASS BOUND AND THE ISGWB SPECTRUM

In the previous section, we had derived a lower mass bound of PBHs originating from a class of USR models of inflation, and also estimated the induced GW energy density coming from the inflection point model we have studied in our previous paper. Both these results have strong dependence on the reheating history between the end of inflation and the start of the RD phase. Our discussion, so far, was limited to an instantaneous reheating. In this section, we shall extend our results by taking into account the effects of a noninstantaneous reheating stage.

### A. Effects of reheating on the lower mass bound

In order to understand the effects of reheating on the PBHs mass bound, we shall first parametrize the reheating phase with an equation of state parameter  $w_{\text{reh}}$  and its duration in number of  $e$ -folds  $N_{\text{reh}}$ . We also assume a sudden transition from the reheating phase to the RD epoch. Following the same arguments as in the previous section, a noninstantaneous reheating epoch shall modify Eq. (3.23), to

$$N_0 - N_p \simeq 47.41 - \frac{1}{4} N_{\text{reh}} (1 - 3w_{\text{reh}}), \quad (4.1)$$

which implies that

$$k_{\text{max}} \simeq 1.94 \times 10^{19} \sigma e^{-\frac{1}{4} N_{\text{reh}} (1 - 3w_{\text{reh}})} \text{ Mpc}^{-1}. \quad (4.2)$$

Note that both  $N_{\text{reh}} = 0$  and  $w_{\text{reh}} = 1/3$  correspond to instantaneous reheating. Since the maximum value of  $k$  shifts to an even lower value, both the lower bound on the PBH mass and the upper bound on the GW frequency become stronger and are given by

$$M_{\text{PBH}} \geq 6.14 \times 10^{-27} \sigma^{-2} e^{\frac{1}{2} N_{\text{reh}} (1 - 3w_{\text{reh}})} M_{\odot}, \quad (4.3)$$

$$f \leq 2.91 \times 10^4 \sigma e^{-\frac{1}{4} N_{\text{reh}} (1 - 3w_{\text{reh}})} \text{ Hz}. \quad (4.4)$$

For  $\sigma \leq 10^{-2}$ ,  $w_{\text{reh}} = 0$ , and  $N_{\text{reh}} = 10$ , these bounds translate to  $M_{\text{PBH}} \geq 9.09 \times 10^{-21} M_{\odot}$  and  $f \leq 23.94 \text{ Hz}$ . Evidently, the lower bounds calculated in the previous section become even stronger in the presence of a nonzero duration of the reheating phase.

### B. Effects of reheating on the ISGWB

To consider the broad effects of different reheating histories on the ISGWB originating from our inflection point inflationary model, we shall assume an effectively sudden transition from the reheating phase to the RD epoch. With this setup, we notice that a noninstantaneous reheating history leaves two very different effects on the observable energy density of the ISGWB.

We have discussed the origin of the first effect in detail in our previous paper [69]. For any inflationary model, different reheating histories change the mapping of different length scales upon their reentry to the horizon, which shifts the peak of the scalar power spectra to lower wavenumbers  $k$  (Fig. 4 of [69]). It also slightly changes the pivot scale normalization, thereby leading to more abundant PBH formation in higher mass range. As the ISGWB involves a convolution integral of first-order scalar power spectra, this shift in the peak of the scalar spectra is reflected as a shift towards lower frequencies in the ISGWB energy density. We found that this effect is strongest for a matter-dominated reheating ( $w_{\text{reh}} = 0$ ), so if we consider the expression of  $\Omega_{\text{GW}}$  as in (2.13), this effect is completely encoded through the primordial scalar power spectra.

The second effect arises due to the nontrivial evolution of scalar perturbation modes and is only significant for an eMD reheating phase. While an eMD epoch leads to a constant transfer function for first-order scalar perturbations, for all subhorizon modes, any other reheating phase (with  $w_{\text{reh}} > 0$ ) would lead to a suppression of the transfer function far before the RD phase starts. A similar suppression for all the subhorizon modes will happen if the transition from the eMD to the RD phase is slow. While we shall not observe any amplification of  $\Omega_{\text{GW}}h^2$  for  $w_{\text{reh}} > 0$  cases and the gradual transition from the eMD to RD phase, a sudden transition from the eMD to RD phase will actually lead to a secondary amplification. For the case of a nearly scale invariant scalar power spectra, this effect is discussed in detail in [97].

In an eMD reheating phase, the first-order scalar perturbations for both the sub- and super-horizon scales stay nearly constant. Just after the transition to the RD phase, the amplitudes of all these modes oscillate rapidly and quickly decay. The oscillation frequency for each mode depends on the corresponding wavenumbers. Both the transfer function  $\mathcal{T}(x, x_r)$  and its time derivative contribute to the term  $f(u, v, x, x_r)$ , as we can see from (A3). For modes with very large wavenumbers which reenter the horizon during the eMD phase, the terms involving the time derivative of  $\mathcal{T}(x, x_r)$  in (A3) contribute dominantly, leading to a secondary amplification of the ISGWB spectra, and the frequency of maximum amplification corresponds to the cutoff scale  $k_{\text{max}}$  of the scalar power spectra. In our case, we take  $k_{\text{max}}$  to be the end of the inflation scale as any scale smaller than this always remains subhorizon and thus no growth can happen for those scales. This effect is essentially encoded in the integral  $I(u, v, x, x_r)$ , as this term covers the time evolution of the source function. We can split the contribution of the  $I$  integral into two parts as

$$I = I_{eMD} + I_{RD}, \quad (4.5)$$

where  $I_{eMD}$  and  $I_{RD}$  are the contributions to the ISGWB produced during eMD and during RD, respectively.

The calculation of  $I_{eMD}$  strongly depends on the gauge choice and recently it has been argued that, during a phase of  $w \leq 0$ , one can neglect this contribution entirely by taking a suitable gauge choice [98]. Also, for the conformal Newtonian gauge, the magnitude arising from  $I_{eMD}$  is sufficiently lower than the contribution of  $I_{RD}$  [97], so in our calculations we neglect any contribution coming from the  $I_{eMD}$  part and focus solely on the contribution from  $I_{RD}$  to the ISGWB produced after the transition to the RD phase.

For the RD phase preceded by an eMD era, an analytical expression of the  $I_{RD}(u, v, x, x_r)$  integral can be obtained after integrating each term by parts. The full analytical expression of  $I(u, v, x, x_r)$  (given in the Appendix) is used to get the ISGWB energy density numerically. We also match the numerical results with the corresponding results in limiting cases  $x_r \ll 1$  and  $x_r \gg 1$ . These two different limits represent the two different peaks quite closely, i.e., the  $x_r \ll 1$  (or  $k \ll k_r$ ) limit corresponds to the pure RD era result and leads to the first peak of the ISGWB in Fig. 4, while the  $x_r \gg 1$  (or  $k \gg k_r$ ) limit correctly represents the second peak. The expressions involving the second limit are derived in (A16) and (A15) of the Appendix, while the expressions for the first limit would reduce to the standard expression (2.14) for the pure RD case.

As seen in the left panel of Fig. 4, any reheating history different than the instantaneous one leads to a shift in the primary peak of the ISGWB power spectra which comes due to the first effect. The second peak only occurs for an eMD reheating, and the frequency of this peak depends on the reheating history. To demonstrate this point, we have also considered the case of  $w_{\text{reh}} = 1/4$ , which is an intermediate state of fluid between the radiation ( $w_{\text{reh}} = 1/3$ ) and the matter ( $w_{\text{reh}} = 0$ ). We found that the second bump does not appear in the case of  $w_{\text{reh}} = 1/4$ , as the behavior of the transfer function in this case is very similar to  $w_{\text{reh}} = 1/3$ . Note that, the frequency of this second resonant peak corresponds to the cutoff scale of the power spectra  $k_{\text{max}}$ , which we can take as the smallest comoving scale leaving the horizon during inflation, or the end of the inflation scale. As we have discussed in the beginning of this section, different reheating histories shall lead to different values of  $k_{\text{max}}$  [c.f. Eq. (4.2)], and thus slightly different values of the second peak frequency. It is this dependence, which is reflected here, in the slight shift in frequency for the second resonant peak in two different durations of the eMD phase. The understanding of the amplitude of the second resonant peak is slightly more complicated, as it depends both on the duration of the reheating phase and also on the amplitude of the primordial scalar power spectra around the cutoff scale, and this amplitude strongly varies as the frequency of the primary peak changes. As we see in the right panel of Fig. 4, for the same duration of the eMD epoch, if we take the power spectra with peaks at two different wavenumbers

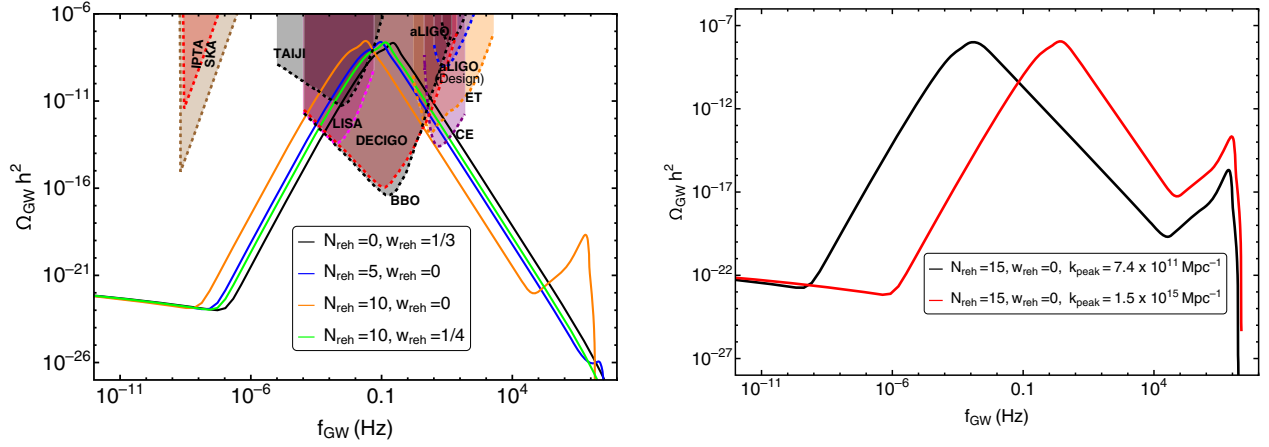


FIG. 4. On the left, the ISGWB energy density  $\Omega_{\text{GW}}h^2$  has been plotted for different reheating histories, as shown in the inset. On the right is the ISGWB energy density for the same reheating history, but for two different scalar power spectra peaking at different wavenumbers  $k$ , leading to the same amplitude at different frequencies for the first peak but different amplitudes at the same frequency for the second peak.

(producing PBHs in two different mass ranges and a primary peak in GW spectra at two different frequencies), the amplifications of the second resonant peak are very different.

## V. CONCLUSIONS AND DISCUSSIONS

In this paper, we have studied the ISGWB from the enhancement of primordial curvature perturbations at smaller scales. An enhancement of the power spectrum is a very generic feature of all the inflationary models, allowing the violation of slow roll conditions [99–101]. In our previous work [69], we had presented an inflationary scenario with a polynomial potential containing an inflection point which can generate PBHs in different mass windows with a nearly monochromatic mass fraction. In particular, PBHs generated in the asteroid mass window are very interesting as they can contribute to all CDM in the universe and the induced GWs have a characteristic peak around the mHz frequency band which can be probed by the future space-based GW observatories such as LISA, DECIGO, or BBO. We have also shown that the secondary GWs induced by more massive PBHs, which will be peaked in the lower frequency range, can be probed by IPTA/SKA observations. Interestingly, in this scenario, we also notice that very light PBHs which may completely evaporate by today and would not contribute to the dark matter at all, will also generate an ISGWB that may be observed from a future design of the ground-based Advanced LIGO detector.

Further, using a model-independent approach, we have obtained a lower bound on the PBH mass by only assuming an instantaneous and a smooth transition from the USR to the SR phase. The lower mass bound of PBHs also becomes stronger in the case of a noninstantaneous reheating epoch. We also investigate the effects of reheating

on the ISGWB spectrum and find that an epoch of noninstantaneous reheating can cause a shift in the GW spectrum to smaller frequencies, thereby making it accessible to the reach of different GW observatories. In particular, we found that a transition from an eMD phase to the RD phase leads to a secondary enhancement of the ISGWB energy density spectrum on much larger frequencies. We stress that our motivation behind the calculation of the lower mass bound is two-fold. First, this mass bound is a model-independent bound and is thus applicable for a large class of USR models, similar to ours. Second, this result has very interesting correlations with our discussion of the very low mass PBH in Sec. II B and its relevance in determining the scales corresponding to the second peak in the induced GW background in the matter-dominated reheating epoch in Sec. IV B. The first step of the lower mass bound calculation is to determine the smallest scale that leaves the horizon just before the end of inflation. It offers us an intuitive way to understand the location of the second GW peak for a matter-dominated reheating. The second step in this calculation is to get a bound on the smallest possible scale leaving the horizon just before the onset of the final slow roll phase such that it leads to a PBH peak in the primordial scalar power spectra. This provides us a lower mass limit on the ultralight PBHs. It also limits how close the first GW peak (corresponding to the PBH scale) can be to the second GW peak (the end of inflation scale). As shown in the right panel of Fig. 4, the amplitude of the second GW peak strongly depends on the proximity to the first GW peak, so this, in principle, also limits the amplitude of the second GW peak.

In general, all cosmological sources of GWs typically produce stochastic backgrounds of GWs with frequencies roughly related to the size of the comoving Hubble horizon at the time of their production. It is worth pointing out that the entire mechanism of PBH generations from scalar field

inflationary models<sup>2</sup> leads to different characteristic backgrounds of GWs which can be distinguished based on their spectral energy density and frequency range.

- (i) Primordial GW backgrounds are from vacuum tensor fluctuations characterized by the tensor to scalar ratio  $r$ . This background is typically very small and highly redshifted since its generation during inflation, and it thus can not be directly detected with present or future GW observatories.
- (ii) Secondary GW backgrounds are sourced by the enhanced scalar perturbations in models of PBH formations. Such GW production is maximized when the scalar modes reenter the horizon during the RD era but decay inside the horizon. This induced contribution typically has a broad peak in the spectra energy density which can be probed with various ground- and space-based GW detectors.
- (iii) The GWs are produced by the mergers of PBH binaries since formation until today [111,112]. The frequency of this GW signal is in the Hz–kHz regime which falls in the sensitivity band of ground-based detectors such as LIGO and future runs such as O5 of Advanced LIGO. Perhaps the binary black hole systems detected by LIGO are PBH binaries. The most recently detected merger event [113] also points to a strong possibility of these intermediate mass black holes origins being primordial [114].
- (iv) The GWs are also produced due to the graviton emission from the Hawking evaporation of PBHs [96]. The emitted GWs from tiny PBHs with high Hawking temperature typically have very high frequencies and are thus quite far from the reach of near future GW observatories.

Recently, it has been discussed whether the spectral energy density of the ISGWB in the RD era from first-order scalar perturbations is gauge invariant. In principle, a physical observable today should not depend on the choice of the gauge in which the calculations are carried out. There have been a few papers discussing this issue lately [115–119], and all of them seem to present different conclusions. All of these papers have computed the spectral energy density of induced gravitational waves in the Newtonian, and the comoving and uniform curvature gauges. In [115], it was noticed that there are huge differences in the final result between the Newtonian and the comoving gauge while the uniform curvature gauge gave the same result as the Newtonian gauge. However, in [116–118] it was claimed that the induced GWs today are

gauge invariant while Ref. [119] claims that the result is identical in four different gauges but still different than other gauges. In summary, the issue of gauge invariance for second-order GWs is not yet completely settled and requires further investigation.

Having computed the power spectrum of induced tensor perturbations, it is interesting and relevant to understand the extent of the induced tensor bispectrum in such models and analyze whether its imprints could possibly be detected by future space-based GW observatories. Recently, it has been pointed out that the non-Gaussianity associated with the induced tensor bispectrum in some models can be large [57,58] and it is imperative to think about the extent of this bispectrum in other inflationary models. Moreover, one can naively expect that all such models which induce a large ISGWB due to the enhancement of primordial curvature perturbations will also generally induce a large tensor bispectrum at the time of GW production, i.e., some time after the horizon reentry of different modes. However, it has been further emphasized that this peculiar non-Gaussian characteristic of the signal may unfortunately not be observable in any GW detectors at present. Since the detectors can only measure the superposition of such signals coming from many different directions in the sky, and not just from one line of sight, such non-Gaussianities (or the phase correlations) would be further decorrelated by the propagation of GWs from different directions due to the inhomogeneities present from their generation epoch to today and thus, will not be observable [57].

It has been pointed out recently that anisotropies in the GW backgrounds are interesting observables that can be used to distinguish among different GW production mechanisms [120,121]. These anisotropies refer to a change in the spectral energy density of observed GWs as a function of direction in the sky and can be imprinted both at the generation epoch as well as, due to their propagation, through the perturbed universe from the formation epoch to today. These anisotropies are similar to the CMB anisotropies and can be computed using a Boltzmann approach, taking into account both the scalar and tensor perturbations [122–124]. Recently, the effects of primordial curvature perturbations on GW propagation over cosmic distances have been calculated and it was shown that the resulting deformations of the GW background can be significant for extremely peaked GW spectra [125]. It will be very interesting to study these anisotropies in the case of scalar induced GW backgrounds and see if they provide further insights into the mechanism of PBH formation and the associated secondary GW background produced in the early universe [126].

Detecting very high frequency GWs is going to be a big challenge for future detectors as high frequencies pose severe complications for interferometric observatories. An interesting thought in this context is based on an indirect

<sup>2</sup>It is well known that dynamical gauge fields during inflation provide very rich and interesting phenomenology [102–108]. In models wherein PBHs are produced due to the amplification of gauge fields, there exists another primordial contribution to tensor perturbations sourced directly by enhanced gauge fields during inflation [109,110].

detection of these high frequency GWs by means of their conversion into electromagnetic (EM) radiation (gravitons  $\rightarrow$  photons) in the presence of a cosmological background magnetic field. This effect is often called the inverse Gertsenshtein effect [127,128]. It has been discussed that relic gravitons emitted by PBHs prior to BBN would transform to an almost isotropic background of electromagnetic radiation due to their conversion [129–131]. This can be calculated at the recombination epoch and during the subsequent evolution of the universe. Since the produced EM radiation is concentrated in the  $x$  ray part of the spectrum, this contribution could be observable and even dominate the cosmic  $x$  ray background. We plan to investigate all such interesting issues in future.

### ACKNOWLEDGMENTS

We would like to thank Chris Byrnes and Ranjan Laha for useful discussions. N. B. thanks Jishnu Sai P and Sahel Dey for fruitful discussions. The financial support from the new faculty seed start-up Grant of IISc, the Core Research Grant No. CRG/2018/002200 from the Science and

Engineering Research Board, Department of Science and Technology, Government of India, and the Infosys Foundation, Bangalore is greatly acknowledged.

### APPENDIX: CALCULATION OF $I_{\text{RD}}(u, v, x, x_r)$ FOR THE RD EPOCH PRECEDED BY AN eMD EPOCH

The general solution for the transfer function in RD, preceded by an eMD phase, can be written as [97]

$$\mathcal{T}(x, x_r) = \frac{3\sqrt{3}[A(x_r)j_1(\frac{x-x_r/2}{\sqrt{3}}) + B(x_r)y_1(\frac{x-x_r/2}{\sqrt{3}})]}{x - x_r/2}, \quad (\text{A1})$$

where  $j_1$  and  $y_1$  are the spherical Bessel functions of first and second kind,  $x_r = k\tau_r$  and  $x = k\tau$ , where  $\tau_r$  corresponds to the conformal time at the transition from the eMD to RD phase,  $\tau$  corresponds to some conformal time after the transition, and  $A, B$  are constants which depend on the duration of the eMD phase. Demanding the continuity of the transfer function  $\mathcal{T}(x)$  and its time derivative at the transition, we can determine  $A$  and  $B$  as

$$\begin{aligned} A(x_r) &= \frac{x_r}{2\sqrt{3}} \sin\left(\frac{x_r}{2\sqrt{3}}\right) - \frac{1}{36}(x_r^2 - 36) \cos\left(\frac{x_r}{2\sqrt{3}}\right), \\ B(x_r) &= -\frac{1}{36}(x_r^2 - 36) \sin\left(\frac{x_r}{2\sqrt{3}}\right) - \frac{x_r}{2\sqrt{3}} \cos\left(\frac{x_r}{2\sqrt{3}}\right), \end{aligned} \quad (\text{A2})$$

where the pure RD case can be recovered by taking the  $x_r \rightarrow 0$  limit. For this general expression of the transfer function, we can calculate  $f(u, v, x)$ ,

$$f(u, v, \bar{x}, x_r) = \frac{4}{9} \left[ (\bar{x} - x_r/2) \partial_{\bar{x}} \mathcal{T}(u\bar{x}, ux_r) ((\bar{x} - x_r/2) \partial_{\bar{x}} \mathcal{T}(v\bar{x}, vx_r) + \mathcal{T}(v\bar{x}, vx_r)) \right] \quad (\text{A3})$$

$$+ \mathcal{T}(u\bar{x}, ux_r) ((\bar{x} - x_r/2) \partial_{\bar{x}} \mathcal{T}(v\bar{x}, vx_r) + 3\mathcal{T}(v\bar{x}, vx_r)) \Big]. \quad (\text{A4})$$

The propagation of GWs shall not be affected by any preceding phase of eMD, so the Green's function for (2.6) shall be same as the pure RD phase, and we can define the integral  $I(u, v, x, x_r)$ , running from the start of the RD  $x_r$  to a later time in the RD phase by which the source term becomes inactive, as

$$I(u, v, x, x_r) = \int_{x_r}^x d\bar{x} \frac{a(\bar{x})}{a(x)} f(u, v, \bar{x}, x_r) kG(\bar{x}, x), \quad (\text{A5})$$

where

$$\frac{a(\bar{x})}{a(x)} = \frac{\bar{x} - x_r/2}{x - x_r/2}. \quad (\text{A6})$$

For simplifying the calculations, we can take  $1/(x - x_r/2)$  out of the integral expression and define

$$\mathcal{I}(u, v, x, x_r) = I(u, v, x, x_r) \times (x - x_r/2). \quad (\text{A7})$$

We can now expand the integrand according to the powers of  $\bar{z} = \bar{x} - x_r/2$ , and integrate it by parts separately to obtain the analytical expression of  $\mathcal{I}(u, v, x, x_r)$ , which can be broken into 6 different terms as

$$\begin{aligned}
\mathcal{I}(u, v, x, x_r) &= \mathcal{I}_s(u, v, x, x_r) \sin(x) + \mathcal{I}_c(u, v, x, x_r) \cos(x) \\
&+ \mathcal{I}_{sm}(u, v, x, x_r) \sin\left(\frac{x(u-v)}{\sqrt{3}}\right) + \mathcal{I}_{sp}(u, v, x, x_r) \sin\left(\frac{x(u+v)}{\sqrt{3}}\right) \\
&+ \mathcal{I}_{cm}(u, v, x, x_r) \cos\left(\frac{x(u-v)}{\sqrt{3}}\right) + \mathcal{I}_{cp}(u, v, x, x_r) \cos\left(\frac{x(u+v)}{\sqrt{3}}\right). \tag{A8}
\end{aligned}$$

To calculate the ISGWB energy density spectra, we need to take the oscillation average of the square of  $\mathcal{I}(u, v, x, x_r)$ . In the late time limit,  $x \gg 1$ , we can neglect all the terms except for the first two terms which simplify the calculation to

$$\overline{\mathcal{I}^2}(u, v, x, x_r) = \frac{1}{2}(\mathcal{I}_s^2(u, v, x, x_r) + \mathcal{I}_c^2(u, v, x, x_r)). \tag{A9}$$

Now, we can further break the  $\mathcal{I}_s(u, v, x, x_r)$  and  $\mathcal{I}_c(u, v, x, x_r)$  terms into two parts, one involving the Si() and Ci() integrals and the other without them:

$$\begin{aligned}
\mathcal{I}_s(u, v, x, x_r) &= \mathcal{I}_{s1}(u, v, x, x_r) + \mathcal{I}_{s2}(u, v, x, x_r), \\
\mathcal{I}_c(u, v, x, x_r) &= \mathcal{I}_{c1}(u, v, x, x_r) + \mathcal{I}_{c2}(u, v, x, x_r). \tag{A10}
\end{aligned}$$

In the  $(x - x_r/2) \gg 1$  limit, using  $\lim_{x \rightarrow \pm\infty} \text{Ci}(x - x_r/2) \rightarrow 0$  and  $\lim_{x \rightarrow \pm\infty} \text{Si}(x - x_r/2) \rightarrow \pm\pi/2$ , we can obtain a simplified expression for these four terms. In this limit, we define  $\text{Si}((-1 + \frac{u+v}{\sqrt{3}})(x - x_r/2)) = \mathcal{V}$ , so that for  $(-1 + \frac{u+v}{\sqrt{3}}) > 0$ ;  $\mathcal{V} = \pi/2$  and for  $(-1 + \frac{u+v}{\sqrt{3}}) < 0$ ;  $\mathcal{V} = -\pi/2$ . These different terms in their simplest form can be expressed as

$$\begin{aligned}
\mathcal{I}_{s1} &= \frac{3}{8u^3v^3}(-3 + u^2 + v^2)^2 \left( - \left( (\pi + 2\mathcal{V})A(vx_r) \left( B(ux_r)\text{Cos}\left(\frac{x_r}{2}\right) + A(ux_r)\text{Sin}\left(\frac{x_r}{2}\right) \right) \right) \right. \\
&- B(vx_r) \left( (\pi + 2\mathcal{V})A(ux_r)\text{Cos}\left(\frac{x_r}{2}\right) + (3\pi - 2\mathcal{V})B(ux_r)\text{Sin}\left(\frac{x_r}{2}\right) \right) \\
&+ 2\text{Ci}\left(\frac{1}{6}(-3 + \sqrt{3}u - \sqrt{3}v)x_r\right) \left( - \left( (A(ux_r)A(vx_r) + B(ux_r)B(vx_r))\text{Cos}\left(\frac{x_r}{2}\right) \right) \right. \\
&+ (A(vx_r)B(ux_r) - A(ux_r)B(vx_r))\text{Sin}\left(\frac{x_r}{2}\right) \left. \right) \\
&+ 2\text{Ci}\left(-\frac{1}{6}(3 + \sqrt{3}u - \sqrt{3}v)x_r\right) \left( - \left( (A(ux_r)A(vx_r) + B(ux_r)B(vx_r))\text{Cos}\left(\frac{x_r}{2}\right) \right) \right. \\
&+ (-A(vx_r)B(ux_r) + A(ux_r)B(vx_r))\text{Sin}\left(\frac{x_r}{2}\right) \left. \right) \\
&+ 2\text{Ci}\left(\frac{1}{6}(-3 + \sqrt{3}u + \sqrt{3}v)x_r\right) \left( (A(ux_r)A(vx_r) - B(ux_r)B(vx_r))\text{Cos}\left(\frac{x_r}{2}\right) \right. \\
&- (A(vx_r)B(ux_r) + A(ux_r)B(vx_r))\text{Sin}\left(\frac{x_r}{2}\right) \left. \right) \\
&+ 2\text{Ci}\left(-\frac{1}{6}(3 + \sqrt{3}u + \sqrt{3}v)x_r\right) \left( (A(ux_r)A(vx_r) - B(ux_r)B(vx_r))\text{Cos}\left(\frac{x_r}{2}\right) \right. \\
&+ (A(vx_r)B(ux_r) + A(ux_r)B(vx_r))\text{Sin}\left(\frac{x_r}{2}\right) \left. \right) + 2 \left( (A(vx_r)B(ux_r) - A(ux_r)B(vx_r))\text{Cos}\left(\frac{x_r}{2}\right) \right. \\
&- (A(ux_r)A(vx_r) + B(ux_r)B(vx_r))\text{Sin}\left(\frac{x_r}{2}\right) \left. \right) \text{Si}\left(\frac{1}{2}\left(-1 - \frac{u}{\sqrt{3}} + \frac{v}{\sqrt{3}}\right)x_r\right) \\
&+ 2 \left( (-A(vx_r)B(ux_r) + A(ux_r)B(vx_r))\text{Cos}\left(\frac{x_r}{2}\right) \right. \\
&- (A(ux_r)A(vx_r) + B(ux_r)B(vx_r))\text{Sin}\left(\frac{x_r}{2}\right) \left. \right) \text{Si}\left(\frac{1}{6}(-3 + \sqrt{3}u - \sqrt{3}v)x_r\right)
\end{aligned}$$

$$\begin{aligned}
& + 2 \left( (A(vx_r)B(ux_r) + A(ux_r)B(vx_r)) \cos\left(\frac{x_r}{2}\right) \right. \\
& + (A(ux_r)A(vx_r) - B(ux_r)B(vx_r)) \sin\left(\frac{x_r}{2}\right) \left. \right) \text{Si}\left(\frac{1}{6}(-3 + \sqrt{3}u + \sqrt{3}v)x_r\right) \\
& + 2 \left( (A(vx_r)B(ux_r) + A(ux_r)B(vx_r)) \cos\left(\frac{x_r}{2}\right) \right. \\
& + (-A(ux_r)A(vx_r) + B(ux_r)B(vx_r)) \sin\left(\frac{x_r}{2}\right) \left. \right) \text{Si}\left(\frac{1}{6}(3 + \sqrt{3}u + \sqrt{3}v)x_r\right), \tag{A11}
\end{aligned}$$

$$\mathcal{I}_{s2} = \frac{1}{36u^2v^2} (3 \cos(x_r)(u^4x_r^2 - 3u^2(x_r^2 + 12) + (v^2 - 3)(v^2x_r^2 - 36)) - x_r \sin(x_r)(u^2(v^2x_r^2 + 54) + 54(v^2 - 3))), \tag{A12}$$

$$\begin{aligned}
\mathcal{I}_{c1} = & \frac{3}{8u^3v^3} (-3 + u^2 + v^2)^2 \left( -B(ux_r) \left( (3\pi - 2\mathcal{V})B(vx_r) \cos\left(\frac{x_r}{2}\right) - (\pi + 2\mathcal{V})A(vx_r) \sin\left(\frac{x_r}{2}\right) \right) \right. \\
& - (\pi + 2\mathcal{V})A(ux_r) \left( A(vx_r) \cos\left(\frac{x_r}{2}\right) - B(vx_r) \sin\left(\frac{x_r}{2}\right) \right) \\
& + 2\text{Ci}\left(\frac{1}{6}(-3 + \sqrt{3}u + \sqrt{3}v)x_r\right) \left( - \left( (A(vx_r)B(ux_r) + A(ux_r)B(vx_r)) \cos\left(\frac{x_r}{2}\right) \right) \right. \\
& + (-A(ux_r)A(vx_r) + B(ux_r)B(vx_r)) \sin\left(\frac{x_r}{2}\right) \left. \right) \\
& + 2\text{Ci}\left(-\frac{1}{6}(3 + \sqrt{3}u + \sqrt{3}v)x_r\right) \left( (A(vx_r)B(ux_r) + A(ux_r)B(vx_r)) \cos\left(\frac{x_r}{2}\right) \right. \\
& + (-A(ux_r)A(vx_r) + B(ux_r)B(vx_r)) \sin\left(\frac{x_r}{2}\right) \left. \right) \\
& + 2\text{Ci}\left(\frac{1}{6}(-3 + \sqrt{3}u - \sqrt{3}v)x_r\right) \left( (A(vx_r)B(ux_r) - A(ux_r)B(vx_r)) \cos\left(\frac{x_r}{2}\right) \right. \\
& + (A(ux_r)A(vx_r) + B(ux_r)B(vx_r)) \sin\left(\frac{x_r}{2}\right) \left. \right) \\
& + 2\text{Ci}\left(-\frac{1}{6}(3 + \sqrt{3}u - \sqrt{3}v)x_r\right) \left( (-A(vx_r)B(ux_r) + A(ux_r)B(vx_r)) \cos\left(\frac{x_r}{2}\right) \right. \\
& + (A(ux_r)A(vx_r) + B(ux_r)B(vx_r)) \sin\left(\frac{x_r}{2}\right) \left. \right) + 2 \left( - \left( (A(ux_r)A(vx_r) + B(ux_r)B(vx_r)) \cos\left(\frac{x_r}{2}\right) \right) \right. \\
& + (-A(vx_r)B(ux_r) + A(ux_r)B(vx_r)) \sin\left(\frac{x_r}{2}\right) \left. \right) \text{Si}\left(\frac{1}{2}\left(-1 - \frac{u}{\sqrt{3}} + \frac{v}{\sqrt{3}}\right)x_r\right) \\
& + 2 \left( - \left( (A(ux_r)A(vx_r) + B(ux_r)B(vx_r)) \cos\left(\frac{x_r}{2}\right) \right) \right. \\
& + (A(vx_r)B(ux_r) - A(ux_r)B(vx_r)) \sin\left(\frac{x_r}{2}\right) \left. \right) \text{Si}\left(\frac{1}{6}(-3 + \sqrt{3}u - \sqrt{3}v)x_r\right) \\
& + 2 \left( (A(ux_r)A(vx_r) - B(ux_r)B(vx_r)) \cos\left(\frac{x_r}{2}\right) \right. \\
& - (A(vx_r)B(ux_r) + A(ux_r)B(vx_r)) \sin\left(\frac{x_r}{2}\right) \left. \right) \text{Si}\left(\frac{1}{6}(-3 + \sqrt{3}u + \sqrt{3}v)x_r\right) \\
& + 2 \left( (-A(ux_r)A(vx_r) + B(ux_r)B(vx_r)) \cos\left(\frac{x_r}{2}\right) \right. \\
& - (A(vx_r)B(ux_r) + A(ux_r)B(vx_r)) \sin\left(\frac{x_r}{2}\right) \left. \right) \text{Si}\left(\frac{1}{6}(3 + \sqrt{3}u + \sqrt{3}v)x_r\right), \tag{A13}
\end{aligned}$$

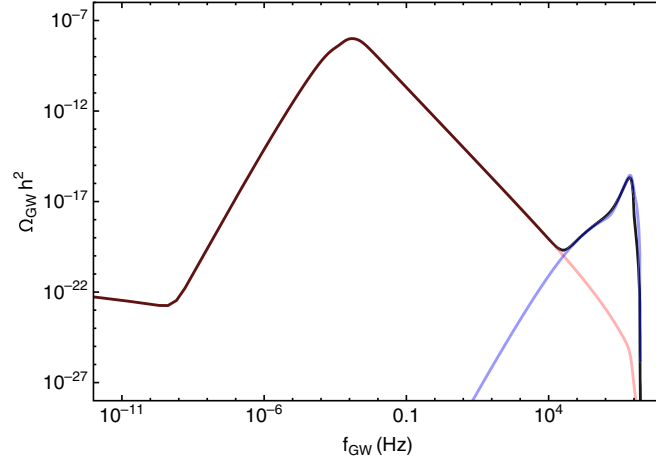


FIG. 5. Comparison of contributions from the pure RD approximation (light red) for the  $k \ll k_r$  limit and from the  $k \gg k_r$  limit result (light blue) along with the full numerical result (solid black).

$$\mathcal{I}_{c2} = -\frac{1}{36u^2v^2} (3 \sin(x_r)(u^4x_r^2 - 3u^2(x_r^2 + 12) + (v^2 - 3)(v^2x_r^2 - 36)) + x_r \cos(x_r)(u^2(v^2x_r^2 + 54) + 54(v^2 - 3))). \quad (\text{A14})$$

Another way of breaking the terms of  $\mathcal{I}_c$  and  $\mathcal{I}_s$  is to identify the terms involving different powers of  $x_r$ . It is possible to show that the term involving the lowest power of  $x_r$  contributes dominantly to the small  $k$  regime ( $k \ll kr$  or  $x_r \ll 1$ ) and reproduces a standard pure RD era formula. This term is also primarily responsible for the first peak in  $\Omega_{\text{GW}} h^2$ , as shown in Fig. 5. The term with highest order of  $x_r$  contributes dominantly for the large  $k$  regime ( $k \gg kr$  or  $x_r \gg 1$ ), and leads to the second peak in Fig. 5. We have also obtained the analytical forms of  $\mathcal{I}_c$  and  $\mathcal{I}_s$  for the large  $k$  regime, which are given below:

$$\begin{aligned} \mathcal{I}_s(x_r \gg 1) \simeq & -\frac{(-3 + u^2 + v^2)^2 x_r^4}{3456uv} \left( 2 \cos\left(\frac{1}{6}(3 + \sqrt{3}u - \sqrt{3}v)x_r\right) \text{Ci}\left(\frac{1}{6}(-3 + \sqrt{3}u - \sqrt{3}v)x_r\right) \right. \\ & + 2 \cos\left(\frac{1}{6}(-3 + \sqrt{3}u - \sqrt{3}v)x_r\right) \text{Ci}\left(-\frac{1}{6}(3 + \sqrt{3}u - \sqrt{3}v)x_r\right) \\ & - 2 \cos\left(\frac{1}{6}(3 + \sqrt{3}u + \sqrt{3}v)x_r\right) \text{Ci}\left(\frac{1}{6}(-3 + \sqrt{3}u + \sqrt{3}v)x_r\right) \\ & - 2 \cos\left(\frac{1}{6}(-3 + \sqrt{3}u + \sqrt{3}v)x_r\right) \text{Ci}\left(-\frac{1}{6}(3 + \sqrt{3}u + \sqrt{3}v)x_r\right) - \pi \sin\left(\frac{1}{6}(-3 + \sqrt{3}u - \sqrt{3}v)x_r\right) \\ & + \pi \sin\left(\frac{1}{6}(3 + \sqrt{3}u - \sqrt{3}v)x_r\right) + \pi \sin\left(\frac{1}{6}(-3 + \sqrt{3}u + \sqrt{3}v)x_r\right) \\ & + 2\mathcal{V} \sin\left(\frac{1}{6}(3 + \sqrt{3}u + \sqrt{3}v)x_r\right) - 2 \sin\left(\frac{1}{6}(-3 + \sqrt{3}u - \sqrt{3}v)x_r\right) \text{Si}\left(\frac{1}{2}\left(-1 - \frac{u}{\sqrt{3}} + \frac{v}{\sqrt{3}}\right)x_r\right) \\ & + 2 \sin\left(\frac{1}{6}(3 + \sqrt{3}u - \sqrt{3}v)x_r\right) \text{Si}\left(\frac{1}{6}(-3 + \sqrt{3}u - \sqrt{3}v)x_r\right) \\ & - 2 \sin\left(\frac{1}{6}(3 + \sqrt{3}u + \sqrt{3}v)x_r\right) \text{Si}\left(\frac{1}{6}(-3 + \sqrt{3}u + \sqrt{3}v)x_r\right) \\ & \left. - 2 \sin\left(\frac{1}{6}(-3 + \sqrt{3}u + \sqrt{3}v)x_r\right) \text{Si}\left(\frac{1}{6}(3 + \sqrt{3}u + \sqrt{3}v)x_r\right) \right), \quad (\text{A15}) \end{aligned}$$

$$\begin{aligned}
\mathcal{I}_c(x_r \gg 1) \simeq & -\frac{(-3+u^2+v^2)^2 x_r^4}{3456uv} \left( \pi \cos\left(\frac{1}{6}(-3+\sqrt{3}u-\sqrt{3}v)x_r\right) \right. \\
& + \pi \cos\left(\frac{1}{6}(3+\sqrt{3}u-\sqrt{3}v)x_r\right) - \pi \cos\left(\frac{1}{6}(-3+\sqrt{3}u+\sqrt{3}v)x_r\right) \\
& + 2\mathcal{V} \cos\left(\frac{1}{6}(3+\sqrt{3}u+\sqrt{3}v)x_r\right) \\
& + 2\text{Ci}\left(-\frac{1}{6}(3+\sqrt{3}u-\sqrt{3}v)x_r\right) \sin\left(\frac{1}{6}(-3+\sqrt{3}u-\sqrt{3}v)x_r\right) \\
& - 2\text{Ci}\left(\frac{1}{6}(-3+\sqrt{3}u-\sqrt{3}v)x_r\right) \sin\left(\frac{1}{6}(3+\sqrt{3}u-\sqrt{3}v)x_r\right) \\
& - 2\text{Ci}\left(-\frac{1}{6}(3+\sqrt{3}u+\sqrt{3}v)x_r\right) \sin\left(\frac{1}{6}(-3+\sqrt{3}u+\sqrt{3}v)x_r\right) \\
& + 2\text{Ci}\left(\frac{1}{6}(-3+\sqrt{3}u+\sqrt{3}v)x_r\right) \sin\left(\frac{1}{6}(3+\sqrt{3}u+\sqrt{3}v)x_r\right) \\
& + 2 \cos\left(\frac{1}{6}(-3+\sqrt{3}u-\sqrt{3}v)x_r\right) \text{Si}\left(\frac{1}{2}\left(-1-\frac{u}{\sqrt{3}}+\frac{v}{\sqrt{3}}\right)x_r\right) \\
& + 2 \cos\left(\frac{1}{6}(3+\sqrt{3}u-\sqrt{3}v)x_r\right) \text{Si}\left(\frac{1}{6}(-3+\sqrt{3}u-\sqrt{3}v)x_r\right) \\
& - 2 \cos\left(\frac{1}{6}(3+\sqrt{3}u+\sqrt{3}v)x_r\right) \text{Si}\left(\frac{1}{6}(-3+\sqrt{3}u+\sqrt{3}v)x_r\right) \\
& \left. + 2 \cos\left(\frac{1}{6}(-3+\sqrt{3}u+\sqrt{3}v)x_r\right) \text{Si}\left(\frac{1}{6}(3+\sqrt{3}u+\sqrt{3}v)x_r\right) \right). \tag{A16}
\end{aligned}$$

- 
- [1] B. P. Abbott *et al.* (LIGO Scientific, Virgo Collaborations), Observation of Gravitational Waves from a Binary Black Hole Merger, *Phys. Rev. Lett.* **116**, 061102 (2016).
- [2] B. Abbott *et al.* (LIGO Scientific, Virgo Collaborations), GW150914: First results from the search for binary black hole coalescence with Advanced LIGO, *Phys. Rev. D* **93**, 122003 (2016).
- [3] B. Abbott *et al.* (LIGO Scientific, Virgo Collaborations), Properties of the Binary Black Hole Merger GW150914, *Phys. Rev. Lett.* **116**, 241102 (2016).
- [4] B. P. Abbott *et al.* (LIGO Scientific, Virgo Collaborations), GW151226: Observation of Gravitational Waves from a 22-Solar-Mass Binary Black Hole Coalescence, *Phys. Rev. Lett.* **116**, 241103 (2016).
- [5] B. P. Abbott *et al.* (LIGO Scientific, Virgo Collaborations), GW170104: Observation of a 50-Solar-Mass Binary Black Hole Coalescence at Redshift 0.2, *Phys. Rev. Lett.* **118**, 221101 (2017); **121**, 129901 (2018).
- [6] B. P. Abbott *et al.* (LIGO Scientific, Virgo Collaborations), GW170814: A Three-Detector Observation of Gravitational Waves from a Binary Black Hole Coalescence, *Phys. Rev. Lett.* **119**, 141101 (2017).
- [7] B. P. Abbott *et al.* (LIGO Scientific, Virgo Collaborations), Astrophysical implications of the binary black-hole merger GW150914, *Astrophys. J.* **818**, L22 (2016).
- [8] K. Belczynski, D. E. Holz, T. Bulik, and R. O’Shaughnessy, The first gravitational-wave source from the isolated evolution of two 40-100 Msun stars, *Nature (London)* **534**, 512 (2016).
- [9] N. Duechting, Supermassive black holes from primordial black hole seeds, *Phys. Rev. D* **70**, 064015 (2004).
- [10] R. Bean and J. Magueijo, Could supermassive black holes be quintessential primordial black holes?, *Phys. Rev. D* **66**, 063505 (2002).
- [11] S. Hawking, Gravitationally collapsed objects of very low mass, *Mon. Not. R. Astron. Soc.* **152**, 75 (1971).
- [12] B. J. Carr and S. W. Hawking, Black holes in the early Universe, *Mon. Not. R. Astron. Soc.* **168**, 399 (1974).
- [13] M. Khlopov, B. A. Malomed, and I. B. Zeldovich, Gravitational instability of scalar fields and formation of primordial black holes, *Mon. Not. R. Astron. Soc.* **215**, 575 (1985).
- [14] P. Ivanov, P. Naselsky, and I. Novikov, Inflation and primordial black holes as dark matter, *Phys. Rev. D* **50**, 7173 (1994).

- [15] J. Garcia-Bellido, A. D. Linde, and D. Wands, Density perturbations and black hole formation in hybrid inflation, *Phys. Rev. D* **54**, 6040 (1996).
- [16] T. Kawaguchi, M. Kawasaki, T. Takayama, M. Yamaguchi, and J. Yokoyama, Formation of intermediate-mass black holes as primordial black holes in the inflationary cosmology with running spectral index, *Mon. Not. R. Astron. Soc.* **388**, 1426 (2008).
- [17] K. Kohri, D. H. Lyth, and A. Melchiorri, Black hole formation and slow-roll inflation, *J. Cosmol. Astropart. Phys.* **04** (2008) 038.
- [18] M. Drees and E. Erfani, Running spectral index and formation of primordial black hole in single field inflation models, *J. Cosmol. Astropart. Phys.* **01** (2012) 035.
- [19] E. Bugaev and P. Klimai, Formation of primordial black holes from non-Gaussian perturbations produced in a waterfall transition, *Phys. Rev. D* **85**, 103504 (2012).
- [20] E. Erfani, Modulated inflation models and primordial black holes, *Phys. Rev. D* **89**, 083511 (2014).
- [21] S. Clesse and J. Garcia-Bellido, Massive primordial black holes from hybrid inflation as dark matter and the seeds of galaxies, *Phys. Rev. D* **92**, 023524 (2015).
- [22] E. Erfani, Primordial black holes formation from particle production during inflation, *J. Cosmol. Astropart. Phys.* **04** (2016) 020.
- [23] J. Garcia-Bellido and E. Ruiz Morales, Primordial black holes from single field models of inflation, *Phys. Dark Universe* **18**, 47 (2017).
- [24] J. M. Ezquiaga, J. Garcia-Bellido, and E. R. Morales, Primordial black hole production in critical Higgs inflation, *Phys. Lett. B* **776**, 345 (2018).
- [25] K. Kannike, L. Marzola, M. Raidal, and H. Veermae, Single field double inflation and primordial black holes, *J. Cosmol. Astropart. Phys.* **09** (2017) 020.
- [26] G. Ballesteros and M. Taoso, Primordial black hole dark matter from single field inflation, *Phys. Rev. D* **97**, 023501 (2018).
- [27] M. P. Hertzberg and M. Yamada, Primordial black holes from polynomial potentials in single field inflation, *Phys. Rev. D* **97**, 083509 (2018).
- [28] S. Pi, Y.-L. Zhang, Q.-G. Huang, and M. Sasaki, Scalaron from  $R^2$ -gravity as a heavy field, *J. Cosmol. Astropart. Phys.* **05** (2018) 042.
- [29] M. Cicoli, V. A. Diaz, and F. G. Pedro, Primordial black holes from string inflation, *J. Cosmol. Astropart. Phys.* **06** (2018) 034.
- [30] A. Y. Kamenshchik, A. Tronconi, T. Vardanyan, and G. Venturi, Non-canonical inflation and primordial black holes production, *Phys. Lett. B* **791**, 201 (2019).
- [31] K. Dimopoulos, T. Markkanen, A. Racioppi, and V. Vaskonen, Primordial black holes from thermal inflation, *J. Cosmol. Astropart. Phys.* **07** (2019) 046.
- [32] V. Atal, J. Cid, A. Escriv, and J. Garriga, PBH in single field inflation: The effect of shape dispersion and non-Gaussianities, *J. Cosmol. Astropart. Phys.* **05** (2020) 022.
- [33] S. S. Mishra and V. Sahni, Primordial black holes from a tiny bump/dip in the inflaton potential, *J. Cosmol. Astropart. Phys.* **04** (2020) 007.
- [34] R.-G. Cai, Z.-K. Guo, J. Liu, L. Liu, and X.-Y. Yang, Primordial black holes and gravitational waves from parametric amplification of curvature perturbations, *J. Cosmol. Astropart. Phys.* **06** (2020) 013.
- [35] D. Y. Cheong, S. M. Lee, and S. C. Park, Primordial black holes in Higgs- $R^2$  inflation as a whole dark matter, *J. Cosmol. Astropart. Phys.* **01** (2021) 032.
- [36] G. Ballesteros, J. Rey, M. Taoso, and A. Urbano, Primordial black holes as dark matter and gravitational waves from single-field polynomial inflation, *J. Cosmol. Astropart. Phys.* **07** (2020) 025.
- [37] G. A. Palma, S. Sypsas, and C. Zenteno, Seeding Primordial Black Holes in Multifield Inflation, *Phys. Rev. Lett.* **125**, 121301 (2020).
- [38] P. Conzino, M. Gasperini, and G. Marozzi, Primordial black holes from pre-big bang inflation, *J. Cosmol. Astropart. Phys.* **08** (2020) 031.
- [39] M. Braglia, D. K. Hazra, F. Finelli, G. F. Smoot, L. Sriramkumar, and A. A. Starobinsky, Generating PBHs and small-scale GWs in two-field models of inflation, *J. Cosmol. Astropart. Phys.* **08** (2020) 001.
- [40] A. A. Starobinsky, Spectrum of relict gravitational radiation and the early state of the universe, *JETP Lett.* **30**, 682 (1979), [http://jetpletters.ru/ps/1370/article\\_20738.shtml](http://jetpletters.ru/ps/1370/article_20738.shtml).
- [41] L. A. Boyle and P. J. Steinhardt, Probing the early universe with inflationary gravitational waves, *Phys. Rev. D* **77**, 063504 (2008).
- [42] R. Durrer and J. Hasenkamp, Testing superstring theories with gravitational waves, *Phys. Rev. D* **84**, 064027 (2011).
- [43] S. Kuroyanagi, T. Chiba, and N. Sugiyama, Prospects for direct detection of inflationary gravitational waves by next generation interferometric detectors, *Phys. Rev. D* **83**, 043514 (2011).
- [44] K. D. Lozanov and M. A. Amin, Equation of State and Duration to Radiation Domination after Inflation, *Phys. Rev. Lett.* **119**, 061301 (2017).
- [45] S. Wang, Y.-F. Wang, Q.-G. Huang, and T. G. F. Li, Constraints on the Primordial Black Hole Abundance from the First Advanced LIGO Observation Run Using the Stochastic Gravitational-Wave Background, *Phys. Rev. Lett.* **120**, 191102 (2018).
- [46] D. G. Figueroa and E. H. Tanin, Ability of LIGO and LISA to probe the equation of state of the early Universe, *J. Cosmol. Astropart. Phys.* **08** (2019) 011.
- [47] M. Guzzetti, N. Bartolo, M. Liguori, and S. Matarrese, Gravitational waves from inflation, *Riv. Nuovo Cimento* **39**, 399 (2016).
- [48] C. Caprini and D. G. Figueroa, Cosmological backgrounds of gravitational waves, *Classical Quantum Gravity* **35**, 163001 (2018).
- [49] K. N. Ananda, C. Clarkson, and D. Wands, The Cosmological gravitational wave background from primordial density perturbations, *Phys. Rev. D* **75**, 123518 (2007).
- [50] D. Baumann, P. J. Steinhardt, K. Takahashi, and K. Ichiki, Gravitational wave spectrum induced by primordial scalar perturbations, *Phys. Rev. D* **76**, 084019 (2007).
- [51] R. Saito and J. Yokoyama, Gravitational Wave Background as a Probe of the Primordial Black Hole Abundance, *Phys. Rev. Lett.* **102**, 161101 (2009); **107**, 069901(E) (2011).
- [52] L. Alabidi, K. Kohri, M. Sasaki, and Y. Sendouda, Observable spectra of induced gravitational waves from inflation, *J. Cosmol. Astropart. Phys.* **09** (2012) 017.

- [53] L. Alabidi, K. Kohri, M. Sasaki, and Y. Sendouda, Observable induced gravitational waves from an early matter phase, *J. Cosmol. Astropart. Phys.* **05** (2013) 033.
- [54] T. Nakama, J. Silk, and M. Kamionkowski, Stochastic gravitational waves associated with the formation of primordial black holes, *Phys. Rev. D* **95**, 043511 (2017).
- [55] K. Kohri and T. Terada, Semianalytic calculation of gravitational wave spectrum nonlinearly induced from primordial curvature perturbations, *Phys. Rev. D* **97**, 123532 (2018).
- [56] R.-g. Cai, S. Pi, and M. Sasaki, Gravitational Waves Induced by non-Gaussian Scalar Perturbations, *Phys. Rev. Lett.* **122**, 201101 (2019).
- [57] N. Bartolo, V. De Luca, G. Franciolini, A. Lewis, M. Peloso, and A. Riotto, Primordial Black Hole Dark Matter: LISA Serendipity, *Phys. Rev. Lett.* **122**, 211301 (2019).
- [58] N. Bartolo, V. De Luca, G. Franciolini, M. Peloso, D. Racco, and A. Riotto, Testing primordial black holes as dark matter with LISA, *Phys. Rev. D* **99**, 103521 (2019).
- [59] K. Inomata and T. Nakama, Gravitational waves induced by scalar perturbations as probes of the small-scale primordial spectrum, *Phys. Rev. D* **99**, 043511 (2019).
- [60] S. Clesse, J. Garcia-Bellido, and S. Orani, Detecting the stochastic gravitational wave background from primordial black hole formation, [arXiv:1812.11011](https://arxiv.org/abs/1812.11011).
- [61] R.-G. Cai, S. Pi, S.-J. Wang, and X.-Y. Yang, Resonant multiple peaks in the induced gravitational waves, *J. Cosmol. Astropart. Phys.* **05** (2019) 013.
- [62] F. Hajkarim and J. Schaffner-Bielich, Thermal history of the early universe and primordial gravitational waves from induced scalar perturbations, *Phys. Rev. D* **101**, 043522 (2020).
- [63] C. Fu, P. Wu, and H. Yu, Scalar induced gravitational waves in inflation with gravitationally enhanced friction, *Phys. Rev. D* **101**, 023529 (2020).
- [64] J. Lin, Q. Gao, Y. Gong, Y. Lu, C. Zhang, and F. Zhang, Primordial black holes and secondary gravitational waves from  $k$  and  $G$  inflation, *Phys. Rev. D* **101**, 103515 (2020).
- [65] G. Domenech, S. Pi, and M. Sasaki, Induced gravitational waves as a probe of thermal history of the universe, *J. Cosmol. Astropart. Phys.* **08** (2020) 017.
- [66] I. Dalianis and K. Kritos, Exploring the spectral shape of gravitational waves induced by primordial scalar perturbations and connection with the primordial black hole scenarios, *Phys. Rev. D* **103**, 023505 (2021).
- [67] H. Ragavendra, P. Saha, L. Sriramkumar, and J. Silk, Primordial black holes and secondary gravitational waves from ultraslow roll and punctuated inflation, *Phys. Rev. D* **103**, 083510 (2021).
- [68] C. Unal, E. D. Kovetz, and S. P. Patil, Multi-messenger probes of inflationary fluctuations and primordial black holes, *Phys. Rev. D* **103**, 063519 (2021).
- [69] N. Bhaumik and R. K. Jain, Primordial black holes dark matter from inflection point models of inflation and the effects of reheating, *J. Cosmol. Astropart. Phys.* **01** (2020) 037.
- [70] K. Danzmann, LISA: An ESA cornerstone mission for a gravitational wave observatory, *Classical Quantum Gravity* **14**, 1399 (1997).
- [71] B. Sathyaprakash and B. Schutz, Physics, astrophysics and cosmology with gravitational waves, *Living Rev. Relativity* **12**, 2 (2009).
- [72] N. Bartolo *et al.*, Science with the space-based interferometer LISA. IV: Probing inflation with gravitational waves, *J. Cosmol. Astropart. Phys.* **12** (2016) 026.
- [73] P. Amaro-Seoane *et al.* (LISA Collaboration), Laser interferometer space antenna, [arXiv:1702.00786](https://arxiv.org/abs/1702.00786).
- [74] W.-H. Ruan, Z.-K. Guo, R.-G. Cai, and Y.-Z. Zhang, Taiji program: Gravitational-wave sources, *Int. J. Mod. Phys. A* **35**, 2050075 (2020).
- [75] N. Seto, S. Kawamura, and T. Nakamura, Possibility of Direct Measurement of the Acceleration of the Universe Using 0.1-Hz Band Laser Interferometer Gravitational Wave Antenna in Space, *Phys. Rev. Lett.* **87**, 221103 (2001).
- [76] K. Yagi and N. Seto, Detector configuration of DECIGO/BBO and identification of cosmological neutron-star binaries, *Phys. Rev. D* **83**, 044011 (2011); **95**, 109901 (E) (2017).
- [77] V. Corbin and N. J. Cornish, Detecting the cosmic gravitational wave background with the big bang observer, *Classical Quantum Gravity* **23**, 2435 (2006).
- [78] J. Aasi *et al.* (LIGO Scientific Collaboration), Advanced LIGO, *Classical Quantum Gravity* **32**, 074001 (2015).
- [79] J. R. Espinosa, D. Racco, and A. Riotto, A cosmological signature of the SM Higgs instability: Gravitational waves, *J. Cosmol. Astropart. Phys.* **09** (2018) 012.
- [80] C. T. Byrnes, P. S. Cole, and S. P. Patil, Steepest growth of the power spectrum and primordial black holes, *J. Cosmol. Astropart. Phys.* **06** (2019) 028.
- [81] P. Carrilho, K. A. Malik, and D. J. Mulryne, Dissecting the growth of the power spectrum for primordial black holes, *Phys. Rev. D* **100**, 103529 (2019).
- [82] J. Chluba, A. L. Erickcek, and I. Ben-Dayan, Probing the inflaton: Small-scale power spectrum constraints from measurements of the CMB energy spectrum, *Astrophys. J.* **758**, 76 (2012).
- [83] C. Germani and I. Musco, Abundance of Primordial Black Holes Depends on the Shape of the Inflationary Power Spectrum, *Phys. Rev. Lett.* **122**, 141302 (2019).
- [84] J. Chluba *et al.*, New horizons in cosmology with spectral distortions of the cosmic microwave background, [arXiv:1909.01593](https://arxiv.org/abs/1909.01593).
- [85] L. Lentati *et al.*, European pulsar timing array limits on an isotropic stochastic gravitational-wave background, *Mon. Not. R. Astron. Soc.* **453**, 2576 (2015).
- [86] R. Shannon *et al.*, Gravitational waves from binary supermassive black holes missing in pulsar observations, *Science* **349**, 1522 (2015).
- [87] A. Kogut, M. Abitbol, J. Chluba, J. Delabrouille, D. Fixsen, J. Hill, S. Patil, and A. Rotti, CMB spectral distortions: Status and prospects, [arXiv:1907.13195](https://arxiv.org/abs/1907.13195).
- [88] B. J. Carr, K. Kohri, Y. Sendouda, and J. Yokoyama, New cosmological constraints on primordial black holes, *Phys. Rev. D* **81**, 104019 (2010).
- [89] B. Carr and F. Kuhnel, Primordial black holes as dark matter: Recent developments, *Annu. Rev. Nucl. Part. Sci.* **70**, 355 (2020).

- [90] R. Laha, Primordial Black Holes as a Dark Matter Candidate Are Severely Constrained by the Galactic Center 511 keV  $\gamma$ -Ray Line, *Phys. Rev. Lett.* **123**, 251101 (2019).
- [91] J. Garcia-Bellido, M. Peloso, and C. Unal, Gravitational wave signatures of inflationary models from primordial black hole dark matter, *J. Cosmol. Astropart. Phys.* **09** (2017) 013.
- [92] B. J. Carr, The Primordial black hole mass spectrum, *Astrophys. J.* **201**, 1 (1975).
- [93] S. J. Kapadia, K. L. Pandey, T. Suyama, and P. Ajith, Prospects for probing ultralight primordial black holes using the stochastic gravitational-wave background induced by primordial curvature perturbations, *Phys. Rev. D* **101**, 123535 (2020).
- [94] J. Liu, Z.-K. Guo, and R.-G. Cai, Analytical approximation of the scalar spectrum in the ultraslow-roll inflationary models, *Phys. Rev. D* **101**, 083535 (2020).
- [95] A. R. Liddle and S. M. Leach, How long before the end of inflation were observable perturbations produced?, *Phys. Rev. D* **68**, 103503 (2003).
- [96] K. Inomata, M. Kawasaki, K. Mukaida, T. Terada, and T. T. Yanagida, Gravitational wave production right after a primordial black hole evaporation, *Phys. Rev. D* **101**, 123533 (2020).
- [97] K. Inomata, K. Kohri, T. Nakama, and T. Terada, Enhancement of gravitational waves induced by scalar perturbations due to a sudden transition from an early matter era to the radiation era, *Phys. Rev. D* **100**, 043532 (2019).
- [98] G. Domènech and M. Sasaki, Approximate gauge independence of the induced gravitational wave spectrum, *Phys. Rev. D* **103**, 063531 (2021).
- [99] R. K. Jain, P. Chingangbam, and L. Sriramkumar, On the evolution of tachyonic perturbations at super-Hubble scales, *J. Cosmol. Astropart. Phys.* **10** (2007) 003.
- [100] R. K. Jain, P. Chingangbam, J.-O. Gong, L. Sriramkumar, and T. Souradeep, Punctuated inflation and the low CMB multipoles, *J. Cosmol. Astropart. Phys.* **01** (2009) 009.
- [101] R. K. Jain, P. Chingangbam, L. Sriramkumar, and T. Souradeep, The tensor-to-scalar ratio in punctuated inflation, *Phys. Rev. D* **82**, 023509 (2010).
- [102] R. Durrer, L. Hollenstein, and R. K. Jain, Can slow roll inflation induce relevant helical magnetic fields?, *J. Cosmol. Astropart. Phys.* **03** (2011) 037.
- [103] C. T. Byrnes, L. Hollenstein, R. K. Jain, and F. R. Urban, Resonant magnetic fields from inflation, *J. Cosmol. Astropart. Phys.* **03** (2012) 009.
- [104] R. K. Jain and M. S. Sloth, Consistency relation for cosmic magnetic fields, *Phys. Rev. D* **86**, 123528 (2012).
- [105] R. K. Jain and M. S. Sloth, On the non-Gaussian correlation of the primordial curvature perturbation with vector fields, *J. Cosmol. Astropart. Phys.* **02** (2013) 003.
- [106] A. Maleknejad, M. Sheikh-Jabbari, and J. Soda, Gauge fields and inflation, *Phys. Rep.* **528**, 161 (2013).
- [107] R. J. Z. Ferreira, R. K. Jain, and M. S. Sloth, Inflationary magnetogenesis without the strong coupling problem, *J. Cosmol. Astropart. Phys.* **10** (2013) 004.
- [108] R. J. Ferreira, R. K. Jain, and M. S. Sloth, Inflationary magnetogenesis without the strong coupling problem II: Constraints from CMB anisotropies and B-modes, *J. Cosmol. Astropart. Phys.* **06** (2014) 053.
- [109] O. Özsoy, Synthetic gravitational waves from a rolling axion monodromy, *J. Cosmol. Astropart. Phys.* **04** (2021) 040.
- [110] O. Özsoy and Z. Lalak, Primordial black holes as dark matter and gravitational waves from bumpy axion inflation, *J. Cosmol. Astropart. Phys.* **01** (2021) 040.
- [111] S. Clesse and J. Garcia-Bellido, Detecting the gravitational wave background from primordial black hole dark matter, *Phys. Dark Universe* **18**, 105 (2017).
- [112] V. Mandic, S. Bird, and I. Cholis, Stochastic Gravitational-Wave Background Due to Primordial Binary Black Hole Mergers, *Phys. Rev. Lett.* **117**, 201102 (2016).
- [113] R. Abbott *et al.* (LIGO Scientific, Virgo Collaborations), GW190521: A Binary Black Hole Merger with a Total Mass of  $150 M_{\odot}$ , *Phys. Rev. Lett.* **125**, 101102 (2020).
- [114] R. Abbott *et al.* (LIGO Scientific, Virgo Collaborations), Properties and astrophysical implications of the  $150 M_{\odot}$  binary black hole merger GW190521, *Astrophys. J. Lett.* **900**, L13 (2020).
- [115] K. Tomikawa and T. Kobayashi, Gauge dependence of gravitational waves generated at second order from scalar perturbations, *Phys. Rev. D* **101**, 083529 (2020).
- [116] V. De Luca, G. Franciolini, A. Kehagias, and A. Riotto, On the gauge invariance of cosmological gravitational waves, *J. Cosmol. Astropart. Phys.* **03** (2020) 014.
- [117] K. Inomata and T. Terada, Gauge independence of induced gravitational waves, *Phys. Rev. D* **101**, 023523 (2020).
- [118] C. Yuan, Z.-C. Chen, and Q.-G. Huang, Scalar induced gravitational waves in different gauges, *Phys. Rev. D* **101**, 063018 (2020).
- [119] Y. Lu, A. Ali, Y. Gong, J. Lin, and F. Zhang, Gauge transformation of scalar induced gravitational waves, *Phys. Rev. D* **102**, 083503 (2020).
- [120] L. Bethke, D. G. Figueroa, and A. Rajantie, Anisotropies in the Gravitational Wave Background from Preheating, *Phys. Rev. Lett.* **111**, 011301 (2013).
- [121] M. Geller, A. Hook, R. Sundrum, and Y. Tsai, Primordial Anisotropies in the Gravitational Wave Background from Cosmological Phase Transitions, *Phys. Rev. Lett.* **121**, 201303 (2018).
- [122] C. R. Contaldi, Anisotropies of gravitational wave backgrounds: A line of sight approach, *Phys. Lett. B* **771**, 9 (2017).
- [123] N. Bartolo, D. Bertacca, S. Matarrese, M. Peloso, A. Ricciardone, A. Riotto, and G. Tasinato, Anisotropies and non-gaussianity of the cosmological gravitational wave background, *Phys. Rev. D* **100**, 121501 (2019).
- [124] N. Bartolo, D. Bertacca, S. Matarrese, M. Peloso, A. Ricciardone, A. Riotto, and G. Tasinato, Characterizing the cosmological gravitational wave background: Anisotropies and non-Gaussianity, *Phys. Rev. D* **102**, 023527 (2020).
- [125] V. Domcke, R. Jinno, and H. Rubira, Deformation of the gravitational wave spectrum by density perturbations, *J. Cosmol. Astropart. Phys.* **06** (2020) 046.
- [126] N. Bartolo, D. Bertacca, V. De Luca, G. Franciolini, S. Matarrese, M. Peloso, A. Ricciardone, A. Riotto, and G. Tasinato, Gravitational wave anisotropies from primordial black holes, *J. Cosmol. Astropart. Phys.* **02** (2020) 028.

- [127] M. Gertsenshtein, Wave resonance of light and gravitational waves, *Sov. Phys. JETP* **14**, 84 (1962).
- [128] Y. B. Zel'dovich, Electromagnetic and gravitational waves in a stationary magnetic field, *Sov. Phys. JETP* **38**, 652 (1974).
- [129] A. D. Dolgov and D. Ejlli, Relic gravitational waves from light primordial black holes, *Phys. Rev. D* **84**, 024028 (2011).
- [130] A. Ejlli, D. Ejlli, A. M. Cruise, G. Pisano, and H. Grote, Upper limits on the amplitude of ultra-high-frequency gravitational waves from graviton to photon conversion, *Eur. Phys. J. C* **79**, 1032 (2019).
- [131] V. Domcke and C. Garcia-Cely, Potential of Radio Telescopes as High-Frequency Gravitational Wave Detectors, *Phys. Rev. Lett.* **126**, 021104 (2021).